On the Diversity of Hybrid Narrowband-PLC/Wireless Communications for Smart Grids

Mostafa Sayed, *Student Member, IEEE,* Theodoros A. Tsiftsis, *Senior Member, IEEE,* and Naofal Al-Dhahir, *Fellow, IEEE*

***Abstract*—Narrowband powerline communications (NB-PLC) and unlicensed wireless communications are two leading communications technologies for the emerging Smart Grid applications. The channel and noise statistics experienced by powerline and wireless transmissions are independent and of a non-identical nature. In this paper, we exploit the diversity provided by the simultaneous transmission of the same information signal over powerline and wireless links to enhance the overall system reliability. In particular, we propose efficient techniques to combine the received signals of the NB-PLC and wireless links for both coherent and differential modulation schemes while considering the impulsive nature of the noise on both links. In addition, we derive closed-form expressions for the average bit-error-rate of the proposed combining techniques. Furthermore, we present simulation results that quantify the performance gains achieved by our proposed receive diversity combining techniques compared to conventional combining techniques.**

***Index Terms*—Impulsive Noise, Powerline Communications, Receive Diversity, Smart Grids, Wireless Communications.**

I. Introduction

Smart Grids are supported by heterogeneous networks that employ both wireless and powerline communication (PLC) technologies since no single solution fits all scenarios [1]. In particular, the two leading contenders for smart-meter two-way wireless communications in the unlicensed $902 - 928$ MHz frequency band in the US are the IEEE 802.15.4g and the emerging IEEE 802.11ah standards. In addition, several PLC standards have been developed for the Smart Grid based on narrowband powerline communication (NB-PLC) in the $3 - 500$ kHz band (e.g. PRIME, G3, IEEE 1901.2, ITU-T G.hnem). NB-PLC is used for last-mile communications between smart meters at the customer sites and data concentrators, which are deployed by local utilities on medium-voltage (MV) or low-voltage (LV) powerlines [2]–[7].

A major design challenge in Smart Grid communications is the presence of strong noise and interference. For instance, in the unlicensed $902 - 928$ MHz band, the wireless interference is primarily generated from uncoordinated transmissions. Non-interoperable neighboring devices, operating in the same frequency band, interfere with each other due to coexistence issues among different standards. Such uncoordinated interference is impulsive in nature and can be characterized by statistical models such as the Gaussian mixture (GM), Middleton Class-A (MCA) and symmetric alpha stable (SαS) models [8]. In NB-PLC, over the unlicensed $3-500$ kHz band, the dominant interference is a combination of narrowband interference and periodic impulsive noise that is synchronous to half of an AC cycle. Typical sources of the noise and interference include non-linear power electronic devices such as inverters, DC-DC converters, and long-wave broadcast stations whose energy is coupled to the powerlines in the $3 - 500$ kHz band. Throughout this paper, we use the term "noise" to refer to the combined effect of both noise and interference.

The use of the unlicensed wireless frequency band for Smart Grid applications is one of the use cases of both the IEEE 802.15.4g and the emerging IEEE 802.11ah standards. For instance, the IEEE 802.11ah standard has included the application of sensors and meters as one of the major use cases [9]–[11]. The coverage of the access point up to 1 km is required whereas at least 100 kbps data rate is assumed for the above use cases. For such application, a 1 MHz bandwidth with a factor of 2 repetition and $1/4$ overall coding rate (including the repetition) is included in the standard so that the transmission range can be increased. The data rate for this scenario is calculated to be 150 kbps [10], [11] including the guard band (25%) and the cyclic prefix (CP) overhead (20%). Hence, for such a case, the bandwidth and the data rate of the wireless link are comparable to those of the NB-PLC link in the $3 - 500$ kHz band. Furthermore, for a 1 MHz channel bandwidth, there are 26 channels in the $902 - 928$ MHz band. In addition, the total bandwidth of the sub-1 GHz band is very narrow compared to the 100 MHz bandwidth in the 2.4 GHz band. Moreover, multiple applications including proprietary ones are operating in the sub-1 GHz band and given the limited number of channels available, these applications might cause high interference to each other. In particular, a critical challenge faced by the IEEE 802.11ah standard is the scarcity of the available spectra in the sub-1 GHz ISM bands [9]. Spatial antenna diversity is a well-known solution to tackle the problem of enhancing the system reliability without sacrificing the spectral efficiency. Similar to antenna diversity, our proposed NB-PLC/wireless

Manuscript received Jul. 27, 2016; revised Feb. 19, 2017; accepted Apr. 7, 2017. Date of publication XXXX XX, 20XX; date of current version XXXX XX, 20XX. The associate editor coordinating the review of this manuscript and approving it for publication was A. Bletsas. This paper was presented in part at the IEEE Global Communications Conference (Globecom), Austin, TX, Dec. 2014 and the IEEE International Conference on Smart Grid Communications (SmartGridComm), Miami, FL, Nov. 2015. This work is supported by a grant from the Semiconductor Research Corporation under SRC GRC Task ID 1836.133 with liaisons Texas Instruments and NXP Semiconductors.

M. Sayed and N. Al-Dhahir are with the Department of Electrical Engineering, University of Texas at Dallas, Richardson, TX 75080 (e-mail: {mostafa.ibrahim, aldhahir}@utdallas.edu).

T. A. Tsiftsis is with the School of Engineering, Nazarbayev University, Astana 010000, Kazakhstan (email: theodoros.tsiftsis@nu.edu.kz).

This article has been accepted for publication in a future issue of this journal, but has not been fully edited. Content may change prior to final publication. Citation information: DOI 10.1109/TWC.2017.2697384, IEEE Transactions on Wireless Communications

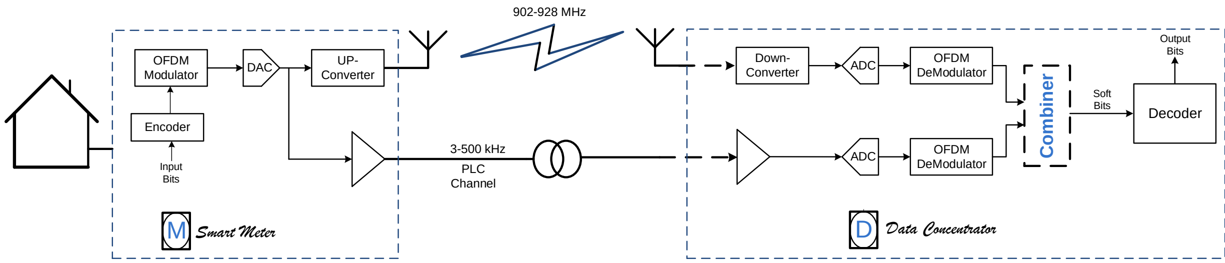

Figure 1. System Block Diagram for NB-PLC/Wireless Diversity.

Table I
KEY VARIABLES USED THROUGHOUT THE PAPER

Variable	Definition	Variable	Definition
l	The OFDM block index	$Y^l_{p,k}$, $Y^l_{w,k}$	The frequency domain received symbol on the NB-PLC and the wireless links, respectively
k	The OFDM subchannel index	$H^l_{p,k}$, $H^l_{w,k}$	The frequency domain channel on the NB-PLC and the wireless links, respectively
N	The total number of OFDM subchannels	$Z^l_{p,k}$, $Z^l_{w,k}$	The frequency domain noise on the NB-PLC and the wireless links, respectively
N'	The number of active OFDM subchannels	σ^2_p, σ^2_w	The average noise power on PLC and wireless links, respectively
L	The number of OFDM blocks within half the AC cycle period	$\tilde{\sigma}^2_{p,lk}$, $\tilde{\sigma}^2_{w,lk}$	The average noise power per subchannel on PLC and wireless links, respectively
N_R	The number of temporal regions for the PLC link noise within half the AC cycle period	$\check{\sigma}^2_{p,lk}$, $\check{\sigma}^2_{w,lk}$	The frequency-domain instantaneous noise power on PLC and wireless links, respectively
M	The number of Gaussian mixture (GM) time-domain noise states on the wireless link	$\sigma^2_{w,m}$	The noise variance of the m-th time-domain GM noise state (out of M states)
X^l_k	The frequency domain transmitted symbol	$\bar{\sigma}^2_{w,i}$	The noise variance of the i-th frequency-domain GM noise state (out of $N+1$ states)

media diversity is also motivated by the need to enhance the system reliability at the same spectral efficiency.

Different from conventional spatial diversity scenarios (e.g. antenna diversity in wireless systems), simultaneous PLC and wireless transmissions experience noise signals with independent and non-identical statistics, which we refer to as an asymmetric diversity scenario. This motivates the need for new receive diversity combining techniques that take into account the asymmetric nature of the noise over the diversity branches. Previous studies on PLC/wireless diversity combining include [12], [13]. However, their investigations considered in-home broadband (BB) PLC transmissions in the $2-30$ MHz band and wireless transmissions in the 2.4 GHz band, assuming MCA noise for the BB-PLC link and additive white Gaussian noise (AWGN) for the wireless link, which have different noise characteristics from those encountered by NB-PLC and wireless communications in the unlicensed $902-928$ MHz band. Furthermore, in [13], the authors presented a comparison between modulation diversity and coding diversity techniques for parallel BB-PLC and wireless transmission in terms of the total throughput. In modulation diversity, the same coded information bits are transmitted over both links while in coding diversity, the coded information bits are demultiplexed over the two links by transmitting half of the information bits over each link. Coding diversity is shown in [13] to achieve a higher throughput than modulation diversity. On the other hand, at the same data rate, modulation diversity achieves a higher diversity gain than coding diversity. In this paper, assuming orthogonal frequency division multiplexing (OFDM) transmission, we propose efficient modulation diversity receive combining techniques for hybrid NB-PLC and unlicensed wireless transmission that are suitable for the asymmetric impulsive characteristics of the noise on both links. It is noteworthy that modulation diversity is a more suitable technique than coding diversity for the proposed hybrid NB-PLC/wireless diversity since reliability (and not high throughput) is the main goal for outdoor smart meter communications. The main contributions of the present paper are summarized as

- For coherent modulation schemes, we propose two receive diversity combining techniques that take into account the asymmetric impulsive nature of the noise on both the PLC and the unlicensed wireless links. The proposed techniques are based on the instantaneous signal-to-noise ratio (SNR) and the noise power spectral density (PSD). The performance of the proposed techniques is compared to the performance of the conventional average-SNR-based combining. The proposed techniques exhibit different performance/complexity tradeoffs.
- For differential modulation schemes, we study the performance of two receive diversity combining techniques, which are the average SNR combining and the equal-gain combining. We show that, since the average SNRs of the two links are not necessarily equal, each one of the two combining techniques is suitable for a certain SNR regime.
- For binary phase-shift keying (BPSK), we derive an uncoded bit-error-rate (BER) expression for the proposed combining techniques for coherent modulation under realistic noise and channel models for both links.
- For differential BPSK (DBPSK), we derive an uncoded BER expression for the PLC link with cyclostationary Gaussian noise and a measurement-based channel model.

- For DBPSK, we derive an uncoded BER expression for the unlicensed wireless link with GM impulsive noise and a Rayleigh fading channel model.
- For DBPSK, we derive an uncoded BER expression for the investigated receive diversity combining techniques for differential modulation.

The remainder of this paper is organized as follows. In the next section, we present the system model including the noise and the channel model assumptions. In Section III, we describe our proposed NB-PLC/wireless receive diversity combining techniques for coherent modulation. In Section IV, we analyze the performance of the proposed coherent modulation combining techniques. In Section V, we describe the proposed differential modulation receive diversity combining techniques. In Section VI, the performance of the proposed differential modulation combining techniques is analyzed. Numerical results are presented in Section VII to compare the performance of the proposed combining techniques. Finally, the paper is concluded in Section VIII. The key variables used in the paper are summarized in Table I.

II. System Model

As shown in Fig. 1, we assume OFDM transmission for both the NB-PLC and wireless links. At the transmit side, the same information signal is sent over both links simultaneously. At the receive side, the received signals from the two links are combined by first calculating the log-likelihood ratios (LLRs or soft bits) for each branch and then adding them using appropriate weights. The combined soft bits are then fed to a detector that applies hard decisions on them to obtain estimates for the transmitted information bits. It is worth noting that the combining is performed at the bit (LLR)-level in order to allow the two links to use different signal constellation sizes, fast Fourier transform (FFT) sizes, cyclic prefix lengths or different sampling rates, as long as both links have the same average bit rate at the combiner input.

The received symbols at the combiner input for the k-th subchannel at the l-th OFDM block for the NB-PLC link, denoted as $Y^l_{p,k}$, and the wireless link, denoted as $Y^l_{w,k}$, are given by $Y^l_{p,k} = H^l_{p,k} X^l_k + Z^l_{p,k}$, $\;Y^l_{w,k} = H^l_{w,k} X^l_k + Z^l_{w,k}$, where X^l_k is the transmitted symbol with variance $E_s = N_b E_b$, where N_b is the number of bits per symbol and E_b is the average energy per bit. $Z^l_{p,k}$ and $Z^l_{w,k}$ are complex random variables (RVs) with zero mean and variances σ^2_p and σ^2_w, respectively, that represent the frequency-domain noise on the NB-PLC and wireless links, respectively. $H^l_{p,k}$ and $H^l_{w,k}$ represent the frequency-domain complex channel coefficients of the PLC and wireless links, respectively. Next, we state and justify our assumptions regarding the noise and the channel models for the NB-PLC and wireless links.

A. NB-PLC Link Noise Model

The generation of the impulsive noise process that best fits actual measurements is presented in [14]. The noise process in NB-PLC is a cyclostationary noise process with a period of half the AC cycle that is divided into N_R temporal regions where the noise over each region can be assumed to be a stationary process. Each region is characterized by a discrete-time linear time-invariant (LTI) filter $h_j(n)$. The average noise power in each region is given by $\mathrm{E}\left(|z(n)|^2\right) = ||h_j(n)||^2,\ n \in \mathcal{I}_j$, where $\mathrm{E}\left(.\right)$ denotes the expectation operation and $\mathcal{I}_j$ denotes the set of indexes of the noise sample that belong to region j. The noise model is then parameterized by: the number of stationary regions N_R, the region intervals $\{\mathcal{I}_j : 1 \le j \le N_R\}$, and the LTI filters $\{h_j(n) : 1 \le j \le N_R\}$, which are represented by their corresponding noise PSDs, denoted by $\{\tilde{\sigma}^2_{p,jk} : 1 \le j \le N_R\}$, obtained from field measurements[1]. Hence, given the noise region index, the probability density function (PDF) of $Z^l_{p,k}$ is Gaussian with zero mean and variance $\tilde{\sigma}^2_{p,lk} = \tilde{\sigma}^2_{p,jk},\ \forall l \in \mathcal{L}_j$, where $\mathcal{L}_j$ denotes the set of OFDM block indexes that belong to the j-th noise region, i.e.

$$Z^l_{p,k}|j \sim \mathcal{CN}\left(0, \tilde{\sigma}^2_{p,jk}\right). \tag{1}$$

σ^2_p can be written in terms of $\tilde{\sigma}^2_{p,jk}$ as $\sigma^2_p = \frac{1}{N'}\sum_{k=0}^{N'-1} \mathcal{R}_1 \tilde{\sigma}^2_{p,1k} + \mathcal{R}_2 \tilde{\sigma}^2_{p,2k} + \mathcal{R}_3 \tilde{\sigma}^2_{p,3k}$, where $\mathcal{R}_j$ denotes the time-percentage of the j-th noise region relative to the noise cyclostationarity period.

B. Wireless Link Noise Model

To the best of the authors' knowledge, there are no papers in the literature that discuss the noise modeling in the $902-928$ MHz (sub-1 GHz) unlicensed wireless band. However, we assumed the analogy between the sub-1 GHz and the 2.4 GHz frequency bands since both are unlicensed bands that have similar operating communication technologies, which are mainly WiFi- or ZigBee-based standards. In particular, ZigBee, Bluetooth, 6LoWPAN, Wi-Fi and RF4CE are widely used 2.4 GHz solutions. Sub-1 GHz standards-based solutions include ZigBee (currently the only protocol offering both 2.4 GHz and sub-1 GHz versions in the 868 MHz and 900 MHz bands), IEEE 802.11ah WiFi standard, EnOcean for automation systems, and ONE-NET for control applications [15], [16]. Hence, we followed the work in [17, Sec 3.3] proposed for the 2.4 GHz band which modeled the noise as a two-component Gaussian mixture random process.

It is well-known that most of the unlicensed wireless standards adopt a random multiple access (MAC) protocol, which avoids collisions by sensing the medium and waiting for random back-off time when there is an ongoing transmission. However, what still causes the interference in this case is the presence of uncoordinated transmissions by non-interoperable devices. In such a case, the devices within the same coverage area might follow different standards, for different applications, that lack coexistence mechanisms between them. An example for such a scenario in the sub-1 GHz band is the presence of devices that follow the IEEE 802.11ah WiFi standard and other non-interoperable devices that follow the IEEE 802.15.4g ZigBee standard, although both standards adopt a carrier sense multiple access (CSMA) with collision avoidance MAC protocol. Furthermore, it is well known that the 2.4 GHz band is currently better in terms of interoperability than the sub-1 GHz since more global standards are being currently introduced for the sub-1 GHz, but most companies deploy proprietary protocols [15], [16].

[1]For more details about the NB-PLC noise generation please refer to [4].

Various statistical models have been proposed to capture the statistics of the noise that affects the uncoordinated wireless transmissions in the unlicensed frequency bands including the GM, the MCA, and the SαS models. Given that the MCA PDF is a special case of the GM PDF and that the SαS RV can also be approximated by a GM RV, we assume that the noise in the wireless link is modeled as a GM random process [8]. Next, we present the time-domain and frequency-domain statistics of the noise on the wireless link.

The PDF of the GM distribution is a weighted sum of a set of Gaussian PDFs. The PDF of a GM RV z is given by $p(z) = \sum_{m=0}^{M-1} \alpha_{w,m}/(\pi\sigma_{w,m}^2) \exp\left(-|z|^2/\sigma_{w,m}^2\right)$, where $\alpha_{w,m}$ is the probability of the m-th Gaussian state, and M is the number of states. Each state has a noise variance $\sigma_{w,m}^2$ where the average noise variance over all states is σ_w^2. We assume that the state with index $m = 0$ represents the thermal noise component. In practice, only two terms of the GM PDF are enough to fit the impulsive noise to the GM model [8].

The noise in the frequency domain is given by $Z_k = 1/\sqrt{N}\sum_{n=0}^{N-1} \zeta_{kn}, \;\; k = 0, \ldots, N-1$, where N is the FFT size and $\zeta_{kn} = z_n \mathrm{e}^{-j\frac{2\pi}{N}kn}$. Given the state of the n-th noise sample, the PDF of ζ_{kn} is Gaussian with zero mean and variance $\sigma_{w,m}^2$, i.e. $\zeta_{kn}|m \sim \mathcal{CN}\left(0, \sigma_{w,m}^2\right)$. Hence, for the special case of $M = 2$, the PDF of Z_k is given by $Z_k \sim \sum_{i=0}^{N} \binom{N}{i} \alpha_{w,0}^i \alpha_{w,1}^{N-i} \mathcal{CN}\left(0, \bar{\sigma}_{w,i}^2\right)$ [18], where $\bar{\sigma}_{w,i}^2 = \dfrac{1}{N}\left[i\sigma_{w,0}^2 + (N-i)\,\sigma_{w,1}^2\right]$. In this case, the PDF of the frequency-domain noise also follows a GM distribution with $N+1$ states. In summary, given the frequency-domain noise state index, the PDF of $Z_{w,k}^l$ is Gaussian with zero mean and variance $\tilde{\sigma}_{w,lk}^2 = \bar{\sigma}_{w,i}^2$. The last statement hold true provided that the N noise samples added to the OFDM block (without CP) of index l have i samples that belong to the first state of the GM distribution (the thermal noise state with prior probability α_o and variance σ_o^2), i.e.

$$Z_{w,k}^l|i \quad \sim \quad \mathcal{CN}\left(0, \bar{\sigma}_{w,i}^2\right). \tag{2}$$

σ_w^2 can be written in terms of $\bar{\sigma}_{w,i}^2$ as $\sigma_w^2 = \sum_{i=0}^{N} \binom{N}{i} \alpha_{w,0}^i \alpha_{w,1}^{N-i} \bar{\sigma}_{w,i}^2$.

C. Channel Models

For the PLC link, we adopt a channel model based on our laboratory measurements for low-voltage (LV) powerline. We measured the channel impulse response (CIR) by sending a known periodic training sequence from one end of the powerline and then estimating the CIR from the received signal at the other end. The measured CIR was found to be periodic with a period of around half of the AC cycle. Similar results for the periodicity of the NB-PLC CIR are reported in [2], [19], [20]. For more details about the measurement-based channel model we adopt in this paper, please refer to [4]. For the wireless link, we assume a Rayleigh fading model since it is widely accepted to capture small-scale fading effects on non-line-of-sight signal propagation in wireless environments.

III. NB-PLC/Wireless Receive Combining For Coherent Modulation

In this section, we highlight the differences between the conventional receive diversity combining scenarios and the proposed NB-PLC/wireless receive diversity, and present our proposed combining techniques for the coherent modulation schemes.

A. Average SNR Combining (ASC)

Given that the noise statistics on both links are asymmetric and that the NB-PLC noise model is non-stationary and is based on field measurements for the noise PSD, it is challenging to derive the optimal maximal ratio combining (MRC) scheme. Furthermore, in the wireless link, the optimal sufficient statistic for signal detection in the presence of GM noise is computationally intensive [21]. A sub-optimal version of the MRC scheme can be implemented by assuming that the noise on both the NB-PLC and wireless links follows a white Gaussian distribution. In this case, the combined log-likelihood (LL) function for the k-th subchannel of the l-th OFDM block can be expressed as

$$\begin{aligned} LL(X_k^l) &= \log\left[p\left(Y_{p,k}^l|H_{p,k}^l X_k^l\right) p\left(Y_{w,k}^l|H_{w,k}^l X_k^l\right)\right] \\ &= -\frac{|Y_{p,k}^l - H_{p,k}^l X_k^l|^2}{\sigma_p^2} - \frac{|Y_{w,k}^l - H_{w,k}^l X_k^l|^2}{\sigma_w^2}, \end{aligned} \tag{3}$$

where σ_p^2 and σ_w^2 are the average noise powers (variances) of the NB-PLC and the wireless links, respectively. Without loss of generality, assuming BPSK modulation, the combined LLR for the k-th subchannel of the l-th OFDM block can be expressed as $LLR_{lk} = LL(X_k^l = 1) - LL(X_k^l = -1) = LLR_{w,lk} + LLR_{p,lk}$. Since the average SNR is inversely proportional to the average noise power, we refer to the combining technique described by (3) as the *average SNR combining* (ASC) technique.

B. Instantaneous SNR Combining (ISC)

From (3), we note that the contribution of each link to the combined LLR is inherently weighted by the inverse of the average noise power on that link. However, due to the impulsive nature of the noise on both the NB-PLC and the wireless links, the noise power level exhibits rapid variations over both time and frequency. As a result, the average noise power can be a highly sub-optimal combining metric for such noise characteristics.

The rapid variations of the instantaneous noise power over the frequency subchannels across several OFDM blocks are evident in Fig. 2. Moreover, the noise power is shown to have a high peak-to-average ratio (PAR), which is higher on the PLC link (around 21 dB) than on the wireless link (around 14 dB). It is worth mentioning that the PAR for the AWGN scenario is around 10 dB. Hence, to capture the instantaneous noise power variations, we propose using the instantaneous noise powers, or equivalently the instantaneous SNRs, as the combining weights. Thus, the LL function can be written as

$$LL_{\text{ISC}}(X_k^l) \quad = \quad -\frac{|Y_{p,k}^l - H_{p,k}^l X_k^l|^2}{\check{\sigma}_{p,lk}^2} - \frac{|Y_{w,k}^l - H_{w,k}^l X_k^l|^2}{\check{\sigma}_{w,lk}^2}, \tag{4}$$

where $\check{\sigma}_{lk}^2$ is the instantaneous noise power for the l-th OFDM block at the k-th subchannel. σ_p^2 and σ_w^2 can be written in terms of $\check{\sigma}_{p,lk}^2$ and $\check{\sigma}_{w,lk}^2$ as $\sigma_p^2 = \mathrm{E}_{l,k}\left[\check{\sigma}_{p,lk}^2\right]$ and $\sigma_w^2 =$

This article has been accepted for publication in a future issue of this journal, but has not been fully edited. Content may change prior to final publication. Citation information: DOI 10.1109/TWC.2017.2697384, IEEE Transactions on Wireless Communications

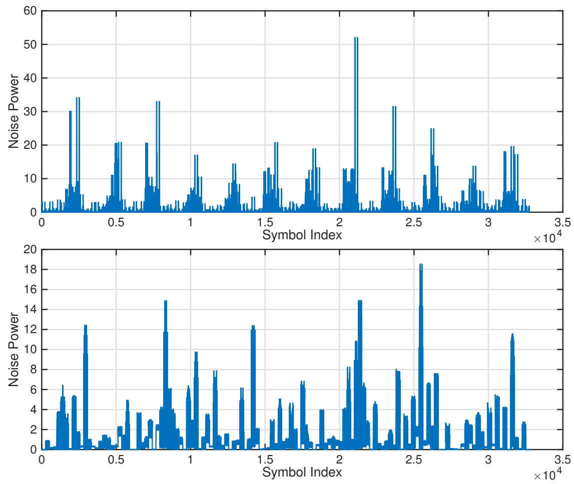

Figure 2. Noise Power in PLC link (top) and wireless link (bottom).

$\mathrm{E}_{l,k}\left[\breve{\sigma}^2_{w,lk}\right]$, respectively, where $\mathrm{E}_{l,k}[.]$ denotes the expectation over the OFDM blocks and the frequency subchannels. To estimate the instantaneous noise power, comb-type pilots can be inserted periodically within the active OFDM subchannels to estimate the noise power at the pilot locations. Then, linear interpolation can be used to estimate the noise power at the non-pilot subchannel locations. More accurate techniques for estimating the instantaneous power of the impulsive noise can be found in the literature. Among others, key papers for cyclostationary impulsive noise power estimation include [3], [22]. However, we believe that comparing the performance of different impulsive noise power estimation techniques is out of the scope of this paper. Nonetheless, we included the performance of the instantaneous SNR combining to show that it has a superior performance to other combining techniques in presence of impulsive noise, as will be shown in the numerical results presented in Section VII.B, and also to motivate future research in impulsive noise power estimation since the available techniques in the literature are either too complex for a practical implementation and/or require very high pilot overhead.

C. PSD Combining (PSDC)

We propose using the average noise power per OFDM subchannel, or equivalently the noise PSD, as the combining metric, since the noise PSD is easier to estimate than the instantaneous noise power. In this case, the LL function can be expressed as

$$\begin{aligned} LL_{\text{PSDC}}(X^l_k) &= -\frac{|Y^l_{p,k}-H^l_{p,k}X^l_k|^2}{\tilde{\sigma}^2_{p,lk}} \\ &- \frac{|Y^l_{w,k}-H^l_{w,k}X^l_k|^2}{\tilde{\sigma}^2_{w,lk}}, \end{aligned} \tag{5}$$

where $\tilde{\sigma}^2_{lk}$ is the average noise power for the l-th OFDM block at the k-th subchannel. It is worth mentioning that the noise PSD might vary from one OFDM block to another in the PLC link since the noise has multiple stationary regions with different PSDs, while for the wireless link the PSD is the same for all OFDM blocks. This is the reason why we added the subscript l to the average noise power per subchannel $\tilde{\sigma}^2_{lk}$. Next, we present a simple and effective technique to estimate the noise PSD from the received signal power.

D. Noise PSD Estimation

The PLC noise is cyclostationary with a period of half the AC cycle. Within each period there are three temporal regions where the PLC noise is stationary over each of them, i.e. the noise PSD is fixed over each of the three regions. Hence, assuming knowledge of the noise region boundaries, the PLC noise PSD for each temporal region can be estimated separately from other regions. In other words, the noise PSD for each noise region is estimated only from the OFDM blocks that belong to this noise region. On the other hand, the wireless link noise, which is assumed to be of GM distribution, is stationary and hence all OFDM blocks can be utilized for noise PSD estimation. Furthermore, the PSD of the noise in the wireless link is shown in the numerical results presented in Section VII.B to be flat over frequency and equal to the GM average noise variance σ^2_w, and hence the noise PSD estimation is not needed for the wireless link. In the following, we explain our proposed noise PSD estimation technique.

The power of the received k-th subchannel of the l-th OFDM block can be written as

$$|Y^l_k|^2 = |H^l_k X^l_k|^2 + |Z^l_k|^2 + 2\mathfrak{Re}\left[H^l_k X^l_k Z^{l*}_k\right]. \tag{6}$$

where $\mathfrak{Re}\,(.)$ denotes the real part operator. Averaging over $|Y^l_k|^2$, we get

$$\begin{aligned} \mathrm{E}\left(|Y^l_k|^2\right) &= \mathrm{E}\left(|H^l_k|^2\right)\mathrm{E}\left(|X^l_k|^2\right) + \mathrm{E}\left(|Z^l_k|^2\right) \\ &+ 2\mathfrak{Re}\left[\mathrm{E}\left(H^l_k X^l_k\right)\mathrm{E}\left(Z^{l*}_k\right)\right]. \end{aligned} \tag{7}$$

Since $\mathrm{E}\left(Z^{l*}_k\right) = 0$, then $\mathrm{E}\left(|Y^l_k|^2\right)$ reduces to $\mathrm{E}\left(|Y^l_k|^2\right) = \mathrm{E}\left(|H^l_k|^2\right)\mathrm{E}\left(|X^l_k|^2\right) + \mathrm{E}\left(|Z^l_k|^2\right)$. Setting $\mathrm{E}\left(|X^l_k|^2\right) = 1$, we get

$$\tilde{\sigma}^2_{lk} = \mathrm{E}\left(|Z^l_k|^2\right) = \mathrm{E}\left(|Y^l_k|^2\right) - \mathrm{E}\left(|H^l_k|^2\right). \tag{8}$$

Hence, from (8), for a certain subchannel k, the noise power can be estimated by subtracting the average channel power from the average received symbol power. Broadly speaking, the averaging length (required for a certain noise PSD estimation accuracy), which is the only parameter for the noise power estimation technique, is dependent on the channel PDF, and the channel autocorrelation function (over time) and its associated channel coherence time in the sense that the averaging length should be long enough such that the channel gain time average approaches $\mathrm{E}\left(|H^l_k|^2\right)$. Furthermore, the averaging time duration has to be long enough to suppress the term $\mathrm{E}\left(Z^{l*}_k\right)$ in (7) to obtain an accurate estimate for the noise PSD. However, the receiver can start decoding the received data, using some initial combining weights, while the averaging is running and does not have to wait for the averaging to converge.

There is an important aspect to note about the channel characteristics in the NB-PLC link. The NB-PLC channel is a deterministic channel, that is either fixed over all OFDM blocks or periodic over one (or half) AC cycle [2]. Hence, for such a case, the averaging of the channel over one AC cycle would be sufficient to obtain the average power for the channel gain per subchannel. However, the averaging length over the received signal power should be longer than one AC cycle

This article has been accepted for publication in a future issue of this journal, but has not been fully edited. Content may change prior to final publication. Citation information: DOI 10.1109/TWC.2017.2697384, IEEE Transactions on Wireless Communications

to ensure that $\mathrm{E}\left(Z_k^{l*}\right) = 0$ and, consequently, that the time average of the received signal power approaches $\mathrm{E}\left(|Y_k^l|^2\right)$.

For PLC noise, the PSD estimation technique can be implemented using three moving-average filters, one for each noise region, where each filter keeps averaging the received frequency domain signal power, following (8), over the filter's corresponding temporal region until this region ends. Once we hit the next region boundary, the next filter is turned on while the currently running filter is paused. Then, we keep multiplexing over the three filters until the convergence of the noise PSD estimation is reached. One method is to terminate the averaging after a certain number of OFDM blocks is reached. Another method is to keep monitoring the change in the estimated noise PSD and terminate the averaging if the change is less than a certain threshold. It is worth mentioning that the current NB-PLC environment is an outdoor environment where the PLC network topology is almost static. Hence, the noise PSD, which depends on the network topology and the connected components within the network, is expected to be fixed. However, in general, we can periodically re-enable the noise PSD estimation to account for any changes in the PLC network. In this case, the re-enable period should be much longer than the noise PSD estimation convergence time. In addition, the PSD combining technique can be set up to use the latest noise PSD estimate until the convergence of the new PSD estimate.

A question that arises here is how to estimate the noise region boundaries. In this regard, in [23], we developed a technique for the noise region boundary estimation and studied its performance in terms of the missed detection rate (MDR) of the noise region boundaries.

IV. Performance Analysis For Coherent Modulation

In this section, first we present analytical expressions for the uncoded average BER for both the PLC and wireless links. Then, we derive an expression for the uncoded average BER of our proposed PSDC technique assuming perfect PSD knowledge. We note that the performance of the ASC technique can be viewed as a special case of the PSDC technique when the noise power is constant over all subchannels. On the other hand, the performance of the ISC technique is dependent on the statistics of the instantaneous noise power, which makes it complex to analyze.

A. PLC Link

The average BER of the PLC link can be written as $P_b\left(E\right) = 1/(LN')\sum_{l=0}^{L-1}\sum_{k=0}^{N'-1} P_{b,k}^l\left(E\right)$, where $P_{b,k}^l\left(E\right)$ is the average BER corresponding to the l-th OFDM block and the k-th subchannel. For BPSK modulation, $P_{b,k}^l\left(E\right)$ is given by $P_{b,k}^l\left(E\right) = Q\left(\sqrt{2\gamma_{p,k}^l}\right)$ [24], where $\gamma_{p,k}^l = E_b|H_{p,k}^l|^2/\tilde{\sigma}_{p,lk}^2$ is the SNR for the k-th subchannel and the l-th OFDM block and $Q\left(.\right)$ is the Gaussian-Q function defined by [24, Eq. (2.3-10)].

B. Wireless Link

The BER of the wireless link can be written as $P_b\left(E\right) = \sum_{i=0}^{N}\binom{N}{i}\alpha_{w,0}^i\alpha_{w,1}^{N-i}P_{b,i}\left(E\right)$, where $P_{b,i}\left(E\right)$, for BPSK modulation and Rayleigh fading, is given by $P_{b,i}\left(E\right) = \frac{1}{2}\Big(1 - \sqrt{\lambda_{w,i}/\left(1+\lambda_{w,i}\right)}\Big)$, where $\lambda_{w,i} = \tilde{E}_{b,h}/\bar{\sigma}_{w,i}^2$, $\tilde{E}_{b,h} = E_bE_h$ and $E_h = \mathrm{E}|H|^2$.

C. NB-PLC/Wireless PSD Combining

Assuming BPSK modulation, the frequency-domain received symbol over the k-th OFDM subchannel and the l-th OFDM block after PSD combining, denoted as $Y_{\mathrm{PSDC},k}^l$, can be represented as[2]

$$\begin{aligned} Y_{\mathrm{PSDC},k}^l &= \left[\frac{|H_{p,k}^l|^2}{\tilde{\sigma}_{p,lk}^2} + \frac{|H_{w,k}^l|^2}{\tilde{\sigma}_{w,lk}^2}\right]X_k^l \\ &+ \left[\frac{\left(H_{p,k}^l\right)^*}{\tilde{\sigma}_{p,lk}^2}Z_{p,k}^l + \frac{\left(H_{w,k}^l\right)^*}{\tilde{\sigma}_{w,lk}^2}Z_{w,k}^l\right]. \end{aligned} \tag{9}$$

The noise term in (9) is complex Gaussian with PDF $\mathcal{CN}\left(0, \left(\gamma_{p,k}^l + \gamma_{w,k}^l\right)/E_b\right)$, where $\gamma_{p,k}^l = E_b|H_{p,k}^l|^2/\tilde{\sigma}_{p,lk}^2$, and $\gamma_{w,k}^l = E_b|H_{w,k}^l|^2/\tilde{\sigma}_{w,lk}^2 = \tilde{E}_{b,h}|H_{w,k}^l|^2/(E_h\bar{\sigma}_{w,i}^2) = |H_{w,k}^l|^2\lambda_{w,i}/E_h$. Hence, the conditional BER given $\gamma_{p,k}^l$ and $\gamma_{w,k}^l$ can be written as $P_{b,k,i}^l\left(E\right) = P_b\left(E|\gamma_{p,k}^l,\gamma_{w,k}^l\right) = Q\left(\sqrt{2\left(\gamma_{p,k}^l+\gamma_{w,k}^l\right)}\right)$. Thus, the PSDC average BER can be expressed as

$$\begin{aligned} P_b\left(E\right) &= \frac{1}{LN'}\sum_{l=0}^{L-1}\sum_{k=0}^{N'-1}\sum_{i=0}^{N}\binom{N}{i}\alpha_{w,0}^i\alpha_{w,1}^{N-i} \\ &\times \int_0^\infty P_{b,k,i}^l\left(E\right)p_{\gamma_{w,i}}\left(t\right)dt, \end{aligned} \tag{10}$$

where $p_{\gamma_{w,i}}\left(t\right) = 1/\lambda_{w,i}\exp\left[-t/\lambda_{w,i}\right]$ assuming a Rayleigh fading channel on the wireless link. Hence, $P_b\left(E\right)$ can be simplified as

$$P_b\left(E\right) = \frac{1}{LN}\sum_{l=0}^{L-1}\sum_{k=0}^{N-1}\sum_{i=0}^{N}\binom{N}{i}\alpha_{w,0}^i\alpha_{w,1}^{N-i}J_{k,i}^l, \tag{11a}$$

$$J_{k,i}^l = \frac{1}{\lambda_{w,i}}\int_0^\infty Q\left(\sqrt{2\left(\gamma_{p,k}^l+t\right)}\right)\exp\left(-\frac{t}{\lambda_{w,i}}\right)dt. \tag{11b}$$

Using integration by parts, $J_{k,i}^l$ can be obtained as

$$\begin{aligned} J_{k,i}^l &= Q\left(\sqrt{2\gamma_{p,k}^l}\right) + 1/(2\sqrt{\pi(1+1/\lambda_{w,i})})\exp\left(\eta_{k,i}^l\right) \\ &\times \Gamma\left(1/2, \eta_{l,k,i} + \gamma_{p,k}^l\right), \end{aligned} \tag{12}$$

where $\eta_{k,i}^l = \gamma_{p,k}^l/\lambda_{w,i}$ and $\Gamma\left(.,.\right)$ is the upper incomplete gamma function defined in [25, Eq. (8.350.2)]. For large values of $\eta_{k,i}^l$, the exponential function in the expression of $J_{k,i}^l$ tends to infinity while the incomplete gamma function tends to zero, which makes $J_{k,i}^l$ indeterminate. To avoid this situation, for high values of $\eta_{k,i}^l$, we evaluate $(J_{k,i}^l)$ using the asymptotic expansion for the upper incomplete gamma function given in [25, Eq. (8.357)]. Hence, (11a) reduces to (see Appendix A for details)

[2] The expression in (9) is the symbol-level combining counterpart to the LLR-level combining expression in (5), where both expressions lead to the same uncoded BER.

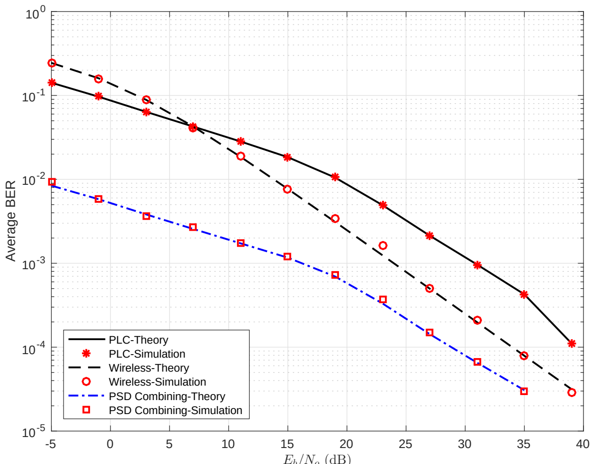

Figure 3. Average BER vs E_b/N_o in dB for BPSK modulation for the PLC link, the wireless link, and the PSDC technique.

$$P_b(E) \approx \begin{cases} \frac{1}{LN}\sum_{l=0}^{L-1}\sum_{k=0}^{N-1}\sum_{i=0}^{N}\binom{N}{i}\alpha_0^i \\ \times\alpha_1^{N-i}J_{k,i}^l,\ \eta_{k,i}^l < \eta_\Gamma^T \\ \frac{1}{LN}\sum_{l=0}^{L-1}\sum_{k=0}^{N-1}\sum_{i=0}^{N}\binom{N}{i}\alpha_0^i \\ \times\alpha_1^{N-i}\tilde{J}_{k,i}^l,\ \eta_{k,i}^l \geq \eta_\Gamma^T \end{cases}, \quad (13a)$$

$$\tilde{J}_{k,i}^l = Q\left(\sqrt{2\gamma_{p,k}^l}\right) + \frac{\exp\left(-\gamma_{p,k}^l\right)}{2\mu_{w,i}\sqrt{\pi\gamma_{p,k}^l}}\left(1-\frac{1}{2\eta_{k,i}^l}\frac{3}{4{\eta_{k,i}^l}^2} - \frac{15}{8{\eta_{k,i}^l}^3}+\frac{105}{16{\eta_{k,i}^l}^4}\right), \quad (13b)$$

where η_Γ^T is set to 50 (see Appendix A for justification). Fig. 3 shows that the derived average BER expressions of the PLC link, the wireless link and the PSD combining match the simulation results. The system parameters used to generate Fig. 3 are listed in Section VII.

V. NB-PLC/Wireless Combining For Differential Modulation

For OFDM transmission, there are two types of differential modulation schemes: frequency-domain differential modulation (FD-DM) and time-domain differential modulation (TD-DM). In FD-DM, the information is carried in the phase difference between two consecutive OFDM subchannels of the same OFDM block. On the other hand, in TD-DM, the information is carried in the phase difference between two OFDM subchannels of two consecutive OFDM blocks at the same frequency subchannel. The performance of FD-DM and TD-DM depends on the channel's frequency and time coherence characteristics, respectively.

Let Y_ν and $Y_{\nu'}$ denote the two received symbols used for the demodulation of the information symbol X_ν. Thus, Y_ν and $Y_{\nu'}$ can be written as $Y_\nu = H_\nu U_\nu + Z_\nu$, $Y_{\nu'} = H_{\nu'}U_{\nu'} + Z_{\nu'}$, where $X_\nu = U_\nu U_{\nu'}^*$, $\nu = lN' + k$, and $\nu' = lN' + k - 1$ or $\nu' = (l-1)N' + k$ for FD-DM and TD-DM, respectively. For differential PSK modulation, a sufficient statistic for symbol detection is given by [24] $\angle D_\nu = \angle\left(Y_\nu Y_{\nu'}^*\right)$, where $\angle(.)$ denotes the angle operation. Assuming the phase difference between H_ν and $H_{\nu'}$ to be very small, D_ν can be approximated as $D_\nu \approxeq |H_\nu||H_{\nu'}|X_\nu + H_{\nu'}^* U_{\nu'}^* Z_\nu + H_\nu U_\nu Z_{\nu'}^* + Z_{\nu'}^* Z_\nu$. In this case, $\angle D_\nu = \angle X_\nu + \phi_\nu$, where ϕ_ν represents the noise term. It is noteworthy that, for differential modulation, channel knowledge is not required for information symbol decoding, and thus pilot transmission is not needed. Let $\hat{D}_\nu = \mathrm{e}^{j\angle D_\nu} = X_\nu + \hat{Z}_\nu$, where $\hat{Z}_\nu$ represents the noise term in $\hat{D}_\nu$, which is assumed to be Gaussian. Hence, we can write the LL function for detecting X_ν as $LL(X_\nu) = -|\hat{D}_\nu - X_\nu|^2$.

Due to the absence of channel knowledge for differential detection, we cannot use receive combining techniques that rely on the received SNR (either the instantaneous SNR or the average SNR per subchannel) since it requires channel knowledge, where the instantaneous SNR and the average SNR per subchannel are defined as $E_s|H_\nu|^2/|Z_\nu|^2$ and $E_s|H_\nu|^2/\tilde{\sigma}_\nu^2$, respectively, where E_s is the variance of U_ν and $U_{\nu'}$. Hence, we consider two alternative techniques for combining the LLRs of the two links; namely, the equal gain combining (EGC) and the ASC techniques, which have the combined LL functions

$$\begin{aligned} LL_{\mathrm{EGC}}(X_\nu) &= LL_p(X_\nu) + LL_w(X_\nu) \\ &= -|\hat{D}_{p,\nu} - X_\nu|^2 - |\hat{D}_{w,\nu} - X_\nu|^2, \end{aligned} \quad (14)$$

$$\begin{aligned} LL_{\mathrm{ASC}}(X_\nu) &= \frac{1}{\sigma_p^2}LL_p(X_\nu) + \frac{1}{\sigma_w^2}LL_w(X_\nu) \\ &= -\frac{1}{\sigma_p^2}|\hat{D}_{p,\nu} - X_\nu|^2 - \frac{1}{\sigma_w^2}|\hat{D}_{w,\nu} - X_\nu|^2. \end{aligned} \quad (15)$$

VI. Performance Analysis For Differential Modulations

In this section, we derive uncoded average BER expressions for differential modulation over the PLC link, the wireless link and the investigated PLC/wireless differential combining techniques, namely, the EGC and ASC techniques.

It follows from Section II that, different from the AWGN model, the noise models for both the NB-PLC and the unlicensed wireless links might cause the two symbols involved in the differential detection to experience noise processes with different variances. Let $\mathbf{R} = [R_1,\ R_2]^t$ represent the two symbols used for the differential detection. Moreover, let $\bar{\mathbf{R}} = \left[\bar{R}_1,\ \bar{R}_2\right]^t$ denote the mean of R and Λ denote the covariance matrix of R, which is defined as

$$\mathbf{\Lambda} = \begin{bmatrix} \sigma_{11} & \sigma_{12} \\ \sigma_{12}^* & \sigma_{22} \end{bmatrix}. \quad (16)$$

Assuming R_1 and R_2 to be jointly Gaussian, their joint PDF can be written as $P(\mathbf{R}) \sim \mathcal{N}(\mathbf{0},\mathbf{\Lambda}) = \pi^{-2}|\Lambda|^{-1}\exp\left[-\left(\mathbf{R}-\bar{\mathbf{R}}\right)^H\mathbf{\Lambda}^{-1}\left(\mathbf{R}-\bar{\mathbf{R}}\right)\right]$. Considering DBPSK modulation and assuming "0" is sent, which means no change in phase, with a zero initial (reference) phase, we can write the optimal detection metric as [24]

$$D_B = \mathfrak{Re}\left(R_1 R_2^*\right). \quad (17)$$

The detection metric in (17) is a special case of the general quadratic detector given by [26] $D = A|R_1|^2 + B|R_2|^2 + CR_1R_2^* + C^*R_1^*R_2$, where $A = B = 0$ and $C = 1/2$ for the differential detector. The average BER of the general quadratic detector is studied in [26] by analyzing the expression $P_b(E;\ \bar{\mathbf{R}},\ \mathbf{\Lambda}) = Pr\left\{D < 0;\ \bar{\mathbf{R}},\ \mathbf{\Lambda}\right\}$. Following a similar analysis to [26], we can write the average BER expression of the detector in (17) in a closed form, which is given by (18), where $Q(a,b)$ is the first-order Marcum Q-function and $I_0(x)$ is the zeroth-order modified Bessel function of the first kind. It is worth noting that the BER expression in (18) is a function of $\bar{\mathbf{R}}$ and $\mathbf{\Lambda}$. Next, we apply the general average BER expression in (18) to the PLC and wireless links.

A. PLC Link

For DBPSK modulation, assuming $X_\nu = 0$ is transmitted, which means no change in phase over the two transmitted symbols carrying X_ν, and assuming the initial phase to be zero, then the received symbols can be written as

$$Y_{p,\nu} = \sqrt{E_b} H_{p,\nu} + Z_{p,\nu},\, Y_{p,\nu'} = \sqrt{E_b} H_{p,\nu'} + Z_{p,\nu'}. \quad (19)$$

Let $\mathbf{Y}_{p,\nu\nu'} = [Y_{p,\nu},\, Y_{p,\nu'}]^t$ with mean $\bar{\mathbf{Y}}_{p,\nu\nu'} = \left[\sqrt{E_b} H_{p,\nu},\, \sqrt{E_b} H_{p,\nu'}\right]^t$ and let $\mathbf{\Lambda}_{p,\nu\nu'}$ denote its covariance matrix which is given by $\mathbf{\Lambda}_{p,\nu\nu'} = \mathrm{diag}\left(\tilde{\sigma}^2_{p,\nu},\, \tilde{\sigma}^2_{p,\nu'}\right)$, where diag(.) forms a diagonal matrix. Let $D_{p,\nu} = \mathfrak{Re}\left(Y_{p,\nu} Y^*_{p,\nu'}\right)$ denote the detection metric. Hence, for both TD- and FD-DM, the average BER is given by

$$P_b(E) = \frac{1}{LN'} \sum_{\nu=0}^{LN'-1} P_{b,\nu\nu'}\left(E;\, \bar{\mathbf{Y}}_{p,\nu\nu'},\, \mathbf{\Lambda}_{p,\nu\nu'}\right), \quad (20)$$

where $P_{b,\nu\nu'}(E) = \Pr\left\{D_{p,\nu} < 0 | X_\nu = 0; \bar{\mathbf{Y}}_{p,\nu\nu'}, \mathbf{\Lambda}_{p,\nu\nu'}\right\}$. Since $P_{b,\nu\nu'}\left(E;\, \bar{\mathbf{Y}}_{p,\nu\nu'},\, \mathbf{\Lambda}_{p,\nu\nu'}\right)$ has the same expression as the BER function given by (18) for $\bar{\mathbf{R}} = \bar{\mathbf{Y}}_{p,\nu\nu'}$ and $\mathbf{\Lambda} = \mathbf{\Lambda}_{p,\nu\nu'}$, $P_{b,\nu\nu'}\left(E;\, \bar{\mathbf{Y}}_{p,\nu\nu'},\, \mathbf{\Lambda}_{p,\nu\nu'}\right)$ can be written as

$$\begin{aligned} P_{b,\nu\nu'}\left(E;\, \bar{\mathbf{Y}}_{p,\nu\nu'},\, \mathbf{\Lambda}_{p,\nu\nu'}\right) &= Q\left(a_{p,\nu\nu'}, b_{p,\nu\nu'}\right) \\ &- \frac{1}{2} I_0\left(a_{p,\nu\nu'} b_{p,\nu\nu'}\right) \exp\Big(-\frac{a^2_{p,\nu\nu'} + b^2_{p,\nu\nu'}}{2}\Big), \end{aligned} \quad (21a)$$

$$a_{p,\nu\nu'} = \sqrt{\frac{E_b}{2} \Big|\frac{H_{p,\nu}}{\tilde{\sigma}_{p,\nu}} - \frac{H_{p,\nu'}}{\tilde{\sigma}_{p,\nu'}}\Big|^2}, \quad (21b)$$

$$b_{p,\nu\nu'} = \sqrt{\frac{E_b}{2} \Big|\frac{H_{p,\nu}}{\tilde{\sigma}_{p,\nu}} + \frac{H_{p,\nu'}}{\tilde{\sigma}_{p,\nu'}}\Big|^2}. \quad (21c)$$

Let

$$\eta_{p,\nu\nu'} = a_{p,\nu\nu'} b_{p,\nu\nu'} = \frac{E_b}{2} \Big| \left[\frac{|H_{p,\nu}|^2}{\tilde{\sigma}^2_{p,\nu}} - \frac{|H_{p,\nu'}|^2}{\tilde{\sigma}^2_{p,\nu'}}\right] \Big|, \quad (22)$$

$$\zeta_{p,\nu\nu'} = \frac{a^2_{p,\nu\nu'} + b^2_{p,\nu\nu'}}{2} = \frac{E_b}{2} \left[\frac{|H_{p,\nu}|^2}{\tilde{\sigma}^2_{p,\nu}} + \frac{|H_{p,\nu'}|^2}{\tilde{\sigma}^2_{p,\nu'}}\right]. \quad (23)$$

Hence, $P_{b,\nu\nu'}\left(E;\, \bar{\mathbf{Y}}_{p,\nu\nu'},\, \mathbf{\Lambda}_{p,\nu\nu'}\right)$ reduces to

$$\begin{aligned} P_{b,\nu\nu'}\left(E;\, \bar{\mathbf{Y}}_{p,\nu\nu'},\, \mathbf{\Lambda}_{p,\nu\nu'}\right) &= Q\left(a_{p,\nu\nu'}, b_{p,\nu\nu'}\right) \\ &- \frac{1}{2} I_0\left(\eta_{p,\nu\nu'}\right) \exp\left(-\zeta_{p,\nu\nu'}\right). \end{aligned} \quad (24)$$

For large values of $\eta_{p,\nu\nu'}$ and $\zeta_{p,\nu\nu'}$, $I_0\left(\eta_{p,\nu\nu'}\right)$ tends to ∞ and $\exp\left(-\zeta_{p,\nu\nu'}\right)$ tends to 0, which makes the quantity $I_0\left(\eta_{p,\nu\nu'}\right) \exp\left(-\zeta_{p,\nu\nu'}\right)$ indeterminate. To overcome this problem, for large values of $\eta_{p,\nu\nu'}$, we use an asymptotic expansion for $I_0\left(\eta_{p,\nu\nu'}\right)$ given in [27, Eq. (10.40.1)]. Hence, (24) reduces to (See Appendix B for details)

$$P_{b,\nu\nu'}\left(E;\, \bar{\mathbf{Y}}_{p,\nu\nu'},\, \mathbf{\Lambda}_{p,\nu\nu'}\right) \approx \begin{cases} Q\left(a_{p,\nu\nu'}, b_{p,\nu\nu'}\right) - \frac{1}{2} \frac{I_0\left(\eta_{p,\nu\nu'}\right)}{\exp\left(\zeta_{p,\nu\nu'}\right)}, & \eta_{p,\nu,\nu'} < \eta^T_{I_0} \\ Q\left(a_{p,\nu\nu'}, b_{p,\nu\nu'}\right) - \frac{1}{2} \exp\left(\tau_{p,\nu\nu'}\right) \kappa_{p,\nu\nu'}, & \eta_{p,\nu,\nu'} \geq \eta^T_{I_0} \end{cases}, \quad (25a)$$

$$\begin{aligned} \tau_{p,\nu\nu'} &= \eta_{p,\nu\nu'} - \zeta_{p,\nu\nu'} \\ &= -E_b \min\left[\frac{|H_{p,\nu}|^2}{\tilde{\sigma}^2_{p,\nu}}, \frac{|H_{p,\nu'}|^2}{\tilde{\sigma}^2_{p,\nu'}}\right], \end{aligned} \quad (25b)$$

$$\begin{aligned} \kappa_{p,\nu\nu'} &= \left(2\pi\eta_{p,\nu\nu'}\right)^{-\frac{1}{2}} \Big[1 + \frac{\eta^{-1}_{p,\nu\nu'}}{8} + \frac{9\eta^{-2}_{p,\nu\nu'}}{128} \\ &+ \frac{225\eta^{-3}_{p,\nu\nu'}}{3072} + \frac{11025\eta^{-4}_{p,\nu\nu'}}{98304}\Big], \end{aligned} \quad (25c)$$

where $\eta^T_{I_0}$ is set to 20 (see Appendix B).

B. Wireless Link

Likewise, for DBPSK modulation, where $X_\nu = 0$ is transmitted and assuming the initial phase to be zero, then $Y_{w,\nu} = \sqrt{E_b} H_{w,\nu} + Z_{w,\nu}$, $Y_{w,\nu'} = \sqrt{E_b} H_{w,\nu'} + Z_{w,\nu'}$, where, $H_{w,\nu}$ and $H_{w,\nu'}$ have a zero-mean complex Gaussian distribution with unit variance and correlation coefficient $\rho = \mathrm{E}\left[H_{w,\nu} H^*_{w,\nu'}\right] / E_h$. Let $D_{w,\nu} = \mathfrak{Re}\left(Y_{w,\nu} Y^*_{w,\nu'}\right)$ denote the detection metric. Let $\mathbf{Y}_{w,\nu\nu'} = [Y_{w,\nu},\, Y_{w,\nu'}]^t$ with mean $\bar{\mathbf{Y}}_{w,\nu\nu'} = [0,\, 0]^t$, since $H_{w,\nu}$, $Z_{w,\nu}$, $H_{w,\nu'}$ and $Z_{w,\nu'}$ have zero means. In addition, let $\mathbf{\Lambda}_{w,\nu\nu'}$ denote the covariance matrix of $\mathbf{Y}_{w,\nu\nu'}$, and hence can be expressed as

$$\begin{aligned} \mathbf{\Lambda}_{w,\nu\nu'} &= \begin{bmatrix} \tilde{E}_{b,h} + \tilde{\sigma}^2_{w,\nu} & \rho \tilde{E}_{b,h} \\ \rho \tilde{E}_{b,h} & \tilde{E}_{b,h} + \tilde{\sigma}^2_{w,\nu'} \end{bmatrix} \\ &= \begin{bmatrix} \tilde{E}_{b,h} + \bar{\sigma}^2_{w,i} & \rho \tilde{E}_{b,h} \\ \rho \tilde{E}_{b,h} & \tilde{E}_{b,h} + \bar{\sigma}^2_{w,i'} \end{bmatrix}, \\ &\forall i, i' \in \{0, \cdots, N\}. \end{aligned} \quad (26)$$

For the TD-DM case, the noise variances over $Y_{w,\nu}$ and $Y_{w,\nu'}$, denoted by $\tilde{\sigma}^2_{w,\nu}$ and $\tilde{\sigma}^2_{w,\nu'}$, might have different values since $Y_{w,\nu}$ and $Y_{w,\nu'}$ belong to two different OFDM blocks over which the noise samples might belong to different GM states. On the other hand, for the FD-DM case, $\tilde{\sigma}^2_{w,\nu} = \tilde{\sigma}^2_{w,\nu'}$ since $Y_{w,\nu}$ and $Y_{w,\nu'}$ belong to the same OFDM block, in general. However, for the special case when $Y_{w,\nu}$ and $Y_{w,\nu'}$ belong to two consecutive OFDM blocks, such that $Y_{w,\nu}$ is the first symbol on the l-th block and $Y_{w,\nu'}$ is the last symbol on the $(l-1)$-th block, $\tilde{\sigma}^2_{w,\nu}$ and $\tilde{\sigma}^2_{w,\nu'}$ might not be equal. Hence, for the DBPSK TD-DM, the average BER of the wireless link can be expressed as $P_b^{TD}(E) = \sum_{i=0}^{N} \sum_{i'=0}^{N} \binom{N}{i} \binom{N}{i'} \alpha_{w,0}^{i+i'} \alpha_{w,1}^{2N-i-i'} P_{b,ii'}(E)$, where $P_{b,ii'}(E) = P_{b,\nu\nu'}(E | \tilde{\sigma}^2_{w,\nu} = \bar{\sigma}^2_{w,i}, \tilde{\sigma}^2_{w,\nu'} = \bar{\sigma}^2_{w,i'}) = \Pr\{D_{w,\nu} < 0 | X_\nu = 0,\, \tilde{\sigma}^2_{w,\nu} = \bar{\sigma}^2_{w,i},\, \tilde{\sigma}^2_{w,\nu'} = \bar{\sigma}^2_{w,i'}\}$. Note that we dropped $\bar{\mathbf{Y}}_{w,\nu\nu'}$ and $\mathbf{\Lambda}_{w,\nu\nu'}$ from being parameters in $P_{b,ii'}(E)$ for simplicity. On the other hand, the average BER for the DBPSK FD-DM can be expressed as $P_b^{FD}(E) = \frac{1}{N'} P_b^{TD}(E) + \frac{N'-1}{N'} \sum_{i=0}^{N} \binom{N}{i} \alpha_{w,0}^{i} \alpha_{w,1}^{N-i} P_{b,ii}(E)$.

The conditional BER $P_{b,ii'}(E)$ can be expressed by the formula in (18) by setting $\bar{\mathbf{R}} = \bar{\mathbf{Y}}_{w,\nu\nu'}$ and $\mathbf{\Lambda} = \mathbf{\Lambda}_{w,\nu\nu'}$ and after simplification it can be written as (see Appendix C for details)

This article has been accepted for publication in a future issue of this journal, but has not been fully edited. Content may change prior to final publication. Citation information: DOI 10.1109/TWC.2017.2697384, IEEE Transactions on Wireless Communications

$$P_b\left(E;\,\bar{\mathbf{R}},\,\mathbf{\Lambda}\right) = \Pr\left\{\mathfrak{Re}\left[R_1R_2^*\right]<0;\,\bar{\mathbf{R}},\,\mathbf{\Lambda}\right\} = Q\left(a,b\right) - \frac{\beta_2/\beta_1}{1+\beta_2/\beta_1}\frac{I_0\left(ab\right)}{\exp\left(\dfrac{a^2+b^2}{2}\right)}, \tag{18}$$

$$a=\sqrt{\frac{2\beta_1^2\beta_2\left(\alpha_1\beta_2-\alpha_2\right)}{\left(\beta_1+\beta_2\right)^2}},\ b=\sqrt{\frac{2\beta_1\beta_2^2\left(\alpha_1\beta_1+\alpha_2\right)}{\left(\beta_1+\beta_2\right)^2}},\ \beta_1=\sqrt{\omega^2+4\xi}-\omega,$$

$$\beta_2=\sqrt{\omega^2+4\xi}+\omega,\ \omega=2\mathfrak{Re}\left(\sigma_{12}\right)\xi,\ \xi=\frac{1}{\sigma_{11}\sigma_{22}-|\sigma_{12}|^2}$$

$$\alpha_1=\frac{1}{4}\left[|\bar{R}_1|^2\sigma_{22}+|\bar{R}_2|^2\sigma_{11}-2\mathfrak{Re}\left(\bar{R}_1\bar{R}_2^*\sigma_{12}\right)\right],\ \alpha_2=\mathfrak{Re}\left(\bar{R}_1\bar{R}_2^*\right)$$

$$P_{b,ii'}\left(E\right) = \frac{1}{2}\left[1-\frac{1}{\sqrt{1+\mu_{w,ii'}}}\right], \tag{27a}$$

$$\mu_{w,ii'}=\frac{1}{\left[\mathfrak{Re}(\rho)\right]^2}\left[\left(1+\bar{\gamma}_{w,i}^{-1}\right)\left(1+\bar{\gamma}_{w,i'}^{-1}\right)-|\rho|^2\right], \tag{27b}$$

where $\bar{\gamma}_{w,i}=\tilde{E}_{b,h}/\bar{\sigma}_{w,i}^2$, $\bar{\gamma}_{w,i'}=\tilde{E}_{b,h}/\bar{\sigma}_{w,i'}^2$. For the special case when the channel correlation coefficient is real, (27a) reduces to

$$P_{b,ii'}\left(E\right)=\frac{1}{2}\left[1-\frac{\rho}{\sqrt{\left(1+\bar{\gamma}_{w,i}^{-1}\right)\left(1+\bar{\gamma}_{w,i'}^{-1}\right)}}\right]. \tag{28}$$

C. NB-PLC/Wireless Combining

For DBPSK, the combined detection metric, denoted by $D_{c,\nu}$, is given by $D_{c,\nu}=g_pD_{p,\nu}+g_wD_{w,\nu}=g_p\mathfrak{Re}(Y_{p,\nu}Y_{p,\nu'}^*)+g_w\mathfrak{Re}(Y_{w,\nu}Y_{w,\nu'}^*)$, where $g_p=g_w=1$ for EGC and $g_p=1/\sigma_p^2$, $g_w=1/\sigma_w^2$ for ASC. As shown in Section VI-B, the average BER expressions of the wireless link for the TD-DM and the FD-DM cases are different since the relations between $\tilde{\sigma}_{w,\nu}^2$ and $\tilde{\sigma}_{w,\nu'}^2$ are different. Similarly, for the NB-PLC/wireless combining, the cases of the TD-DM and the FD-DM for the wireless link have different average BER expressions. For TD-DM for the wireless link, the uncoded average BER is given by

$$P_b^{TD}\left(E\right) = \frac{1}{LN'}\sum_{i=0}^{N}\sum_{i'=0}^{N}\binom{N}{i}\binom{N}{i'}\alpha_{w,0}^{i+i'}\,\alpha_{w,1}^{2N-i-i'} \times \sum_{\nu=0}^{LN'-1}P_{b,\nu,i}\left(E\right), \tag{29}$$

where we dropped the subscripts ν' and i' in $P_{b,\nu,i}\left(E\right)$ for simplicity. Moreover, we dropped $\bar{\mathbf{Y}}_{p,\nu\nu'}$, $\mathbf{\Lambda}_{p,\nu\nu'}$, $\bar{\mathbf{Y}}_{w,\nu\nu'}$ and $\mathbf{\Lambda}_{w,\nu\nu'}$ from being parameters in $P_{b,\nu,i}\left(E\right)$ for simplicity. For FD-DM for the wireless link, the uncoded average BER is given by

$$P_b^{FD}\left(E\right) = \frac{1}{N'}P_b^{TD}\left(E\right)+\frac{N'-1}{N'}\sum_{i=0}^{N}\binom{N}{i}\alpha_{w,0}^{i}\alpha_{w,1}^{N-i} \times \frac{1}{LN'}\sum_{\nu=0}^{LN'-1}P_{b,\nu,ii}\left(E\right), \tag{30}$$

where $P_{b,\nu,ii}=P_{b,\nu,i}\left(E\right)$ with $i'=i$. The conditional BER $P_{b,\nu,i}\left(E\right)$ can be evaluated as the probability that $D_{c,\nu}<0|X_\nu=0$. Hence, $P_{b,\nu,i}\left(E\right)$ can be written in terms of the moment generating function (MGF) of $D_{c,\nu}$ as $P_{b,\nu,i}\left(E\right)=-1/(2\pi j)\int_{-i\infty-\epsilon}^{i\infty-\epsilon}\psi_{D_{c,\nu}}\left(v\right)/v\,dv$, where ϵ is a real number chosen to move the integration path away from the singularities [26]. The MGFs of $g_pD_{p,\nu}$ and $g_wD_{w,\nu}$ can be obtained from the MGF of the general quadratic form reported in [26]. The MGF of $D_{c,\nu}$ can be obtained as the product of the MGFs of $g_pD_{p,\nu}$ and $g_wD_{w,\nu}$ since both are independent. Hence, using the MGF of $D_{c,\nu}$, a closed-form expression for $P_{b,\nu,i}\left(E\right)$ is derived. The derived expression is given by (31a), where $I_n(x)$ is the n-th order modified Bessel function of the first kind. The details of the derivation of the $P_{b,\nu,i}\left(E\right)$ expression are shown in Appendix D. The expression in (31a) is only valid when $\beta_{p,\nu}\neq\beta_{w,2,i}$. On the other hand, for the special case when $\beta_{p,\nu}=\beta_{w,2,i}$, $P_{b,\nu,i}\left(E\right)$ can be written as

$$P_{b,\nu,i}\left(E\right) = \frac{\frac{1}{2}\beta_{w,1,i}\beta_{w,2,i}}{\left(\beta_{w,1,i}+\beta_{p,\nu}\right)\left(\beta_{w,2,i}+\beta_{p,\nu}\right)}\left[\tilde{c}_{0,\nu,i}J_{0,\nu} + \tilde{c}_{1,\nu,i}J_{1,\nu}+\tilde{c}_{2,\nu,i}J_{2,\nu,i}+\tilde{J}_{3,\nu}\right], \tag{32a}$$

$$\tilde{c}_{0,\nu,i}=1-\tau_{1,\nu,i},\ \tilde{c}_{1,\nu,i}=\frac{1}{1+\tau_{1,\nu,i}},\ \tilde{c}_{2,\nu,i}=\frac{\tau_{1,\nu,i}^2}{1+\frac{1}{\tau_{1,\nu,i}}},$$

$$\tilde{J}_{3,\nu}=\sum_{n=0}^{3}\frac{\binom{3}{n}I_{|n-1|}(\eta_\nu)}{\left(\frac{a_\nu}{b_\nu}\right)^{1-n}\exp\left(\zeta_\nu\right)}. \tag{32b}$$

Similar to (24), the term $I_m\left(\eta\right)\exp\left(-\zeta\right)$ becomes indeterminate at large values of η and ζ. Hence, for large values of η, we use an asymptotic expansion for $I_m\left(\eta\right)$ given in [27, Eq. (10.40.1)]. Thus, for $\eta>\eta_I^T$, $I_m\left(\eta\right)\exp\left(-\zeta\right)$ can be approximated as

$$I_m(\eta)\exp\left(-\zeta\right)\approx\frac{\exp\left(\eta-\zeta\right)}{\sqrt{2\pi\eta}}\sum_{s=0}^{M_I^L-1}\frac{\left(-1\right)^s a_s(m)}{s!\left(8\eta\right)^s},\ \eta>\eta_I^T, \tag{33a}$$

$$a_0(m) = 1,\ a_s(m)=\left(4m^2-1^2\right)\left(4m^2-3^2\right)\ldots\left(4m^2-(2s-1)^2\right),\ s\geq 1, \tag{33b}$$

where M_I^L is set to 10 terms and η_I^T is set to 40 to achieve a normalized root mean squared error (NRMSE) for the approximation that is less than 10^{-7}. Moreover, since the evaluation of the Bessel functions and the Marcum-Q function might be time-consuming, series expansions for these functions can be used as approximations. An accurate approximation for the Bessel functions with small arguments, $\eta\leq\eta_I^T$, is given in [25] as $I_m(\eta)\approx\sum_{s=0}^{M_I^S-1}\frac{\left(\frac{\eta}{2}\right)^{m+2s}}{s!\Gamma(m+s+1)}$, $\eta\leq\eta_I^T$, where M_I^S is set to 35 terms to achieve an NRMSE less than 10^{-7}, and $\Gamma\left(.\right)$ is the gamma function. In addition, for small arguments, the Marcum-Q function can be approximated as [28]

$$Q\left(a,b\right) \approx \sum_{m=0}^{M_Q^S-1}\sum_{s=0}^{m}\frac{a^{2m}b^{2s}}{m!s!2^{m+s}}\exp\left(-\frac{a^2+b^2}{2}\right),\quad \eta=ab\leq\eta_Q^T, \tag{34}$$

This article has been accepted for publication in a future issue of this journal, but has not been fully edited. Content may change prior to final publication. Citation information: DOI 10.1109/TWC.2017.2697384, IEEE Transactions on Wireless Communications

$$P_{b,\nu,i}\left(E\right) = \frac{\beta_{w,1,i}\beta_{w,2,i}}{2\left(\beta_{w,1,i}+\beta_{p,\nu}\right)\left(\beta_{w,2,i}-\beta_{p,\nu}\right)}\left[J_{0,\nu}+c_{1,\nu,i}J_{1,\nu}+c_{2,\nu,i}J_{2,\nu,i}+c_{3,\nu,i}J_{3,\nu,i}\right], \tag{31a}$$

$$\beta_{w,1,i} = \sqrt{\omega_{w,i}^2+\frac{4\xi_{w,i}}{g_w^2}}-\omega_{w,i},\ \beta_{w,2,i} = \sqrt{\omega_{w,i}^2+\frac{4\xi_{w,i}}{g_w^2}}+\omega_{w,i}, \tag{31b}$$

$$\xi_{w,i} = \left[(\tilde{E}_{b,h}+\bar{\sigma}_{w,i}^2)(\tilde{E}_{b,h}+\bar{\sigma}_{w,i'}^2)-|\rho\tilde{E}_{b,h}|^2\right]^{-1},\ \omega_{w,i} = \frac{2\mathfrak{Re}\left[\rho\tilde{E}_{b,h}\right]\xi_{w,i}}{g_w}, \tag{31c}$$

$$\beta_{p,\nu} = \frac{2}{g_p\tilde{\sigma}_{p,\nu}\tilde{\sigma}_{p,\nu'}},\ a_\nu = \sqrt{\frac{\beta_{p,\nu}}{2}\left[\alpha_{p,1,\nu}\beta_{p,\nu}-\alpha_{p,2,\nu}\right]},\ b_\nu = \sqrt{\frac{\beta_{p,\nu}}{2}\left[\alpha_{p,1,\nu}\beta_{p,\nu}+\alpha_{p,2,\nu}\right]}, \tag{31d}$$

$$\alpha_{p,1,\nu} = \frac{g_p^2E_b}{4}\left[|H_{p,\nu}|^2\tilde{\sigma}_{p,\nu'}^2+|H_{p,\nu'}|^2\tilde{\sigma}_{p,\nu}^2\right],\ \alpha_{p,2,\nu} = g_pE_b\mathfrak{Re}\left[H_{p,\nu}H_{p,\nu'}^*\right], \tag{31e}$$

$$c_{1,\nu,i} = \frac{1}{(1+\tau_{1,\nu,i})(1+\tau_{2,\nu,i})},\ c_{2,\nu,i} = \frac{-\tau_{1,\nu,i}}{(1+\frac{1}{\tau_{1,\nu,i}})(1-\frac{\tau_{2,\nu,i}}{\tau_{1,\nu,i}})},\ c_{3,\nu,i} = \frac{-\tau_{2,\nu,i}}{(1+\frac{1}{\tau_{2,\nu,i}})(1-\frac{\tau_{1,\nu,i}}{\tau_{2,\nu,i}})}, \tag{31f}$$

$$\tau_{1,\nu,i} = \frac{\beta_{w,1,i}-\beta_{p,\nu}}{\beta_{w,1,i}+\beta_{p,\nu}},\ \tau_{2,\nu,i} = \frac{\beta_{w,2,i}+\beta_{p,\nu}}{\beta_{w,2,i}-\beta_{p,\nu}},\ \eta_\nu = a_\nu b_\nu,\ \zeta_\nu = \frac{a_\nu^2+b_\nu^2}{2}, \tag{31g}$$

$$\hat{a}_{\nu,i} = a_\nu\sqrt{|\tau_{1,\nu,i}|},\ \hat{b}_{\nu,i} = \frac{b_\nu}{\sqrt{|\tau_{1,\nu,i}|}},\ \check{a}_{\nu,i} = a_\nu\sqrt{|\tau_{2,\nu,i}|},\ \check{b}_{\nu,i} = \frac{b_\nu}{\sqrt{|\tau_{2,\nu,i}|}}, \tag{31h}$$

$$\hat{\eta}_{\nu,i} = \hat{a}_{\nu,i}\hat{b}_{\nu,i},\ \hat{\zeta}_{\nu,i} = \frac{\hat{a}_{\nu,i}^2+\hat{b}_{\nu,i}^2}{2}, \check{\eta}_{\nu,i} = \check{a}_{\nu,i}\check{b}_{\nu,i},\ \check{\zeta}_{\nu,i} = \frac{\check{a}_{\nu,i}^2+\check{b}_{\nu,i}^2}{2}, \tag{31i}$$

$$J_{0,\nu} = \sum_{n=0}^{3}\binom{3}{n}\left(\frac{a_\nu}{b_\nu}\right)^n\frac{I_n(\eta_\nu)}{\exp\left(\zeta_\nu\right)},\ J_{1,\nu} = \sum_{n=0}^{3}\binom{3}{n}\left[Q_1\left(a_\nu,b_\nu\right)-\sum_{m=0}^{n}\left(\frac{a_\nu}{b_\nu}\right)^m\frac{I_m(\eta_\nu)}{\exp\left(\zeta_\nu\right)}\right], \tag{31j}$$

$$J_{2,\nu,i} = \begin{cases}\sum_{n=0}^{3}\frac{\binom{3}{n}\exp\left(\hat{\zeta}_{\nu,i}\right)}{|\tau_{1,\nu,i}|^{n+1}\exp(\zeta_\nu)}\left[Q_1\left(\hat{a}_{\nu,i},\hat{b}_{\nu,i}\right)-\sum_{m=0}^{n}\left(\frac{\hat{a}_{\nu,i}}{\hat{b}_{\nu,i}}\right)^m\frac{I_m(\hat{\eta}_{\nu,i})}{\exp(\hat{\zeta}_{\nu,i})}\right], & -1<\tau_{1,\nu,i}<0\\ \sum_{n=0}^{3}\frac{\binom{3}{n}\exp\left(\hat{\zeta}_{\nu,i}\right)}{(-\tau_{1,\nu,i})^{n+1}\exp(\zeta_\nu)}\sum_{m=n+1}^{\infty}\left(-\frac{\hat{a}_{\nu,i}}{\hat{b}_{\nu,i}}\right)^m\frac{I_m(\hat{\eta}_{\nu,i})}{\exp\left(\hat{\zeta}_{\nu,i}\right)}, & 0<\tau_{1,\nu,i}<1\end{cases}, \tag{31k}$$

$$J_{3,\nu,i} = \begin{cases}\sum_{n=0}^{3}\frac{-\binom{3}{n}\exp(\check{\zeta}_{\nu,i})Q_1(\check{b}_{\nu,i},\check{a}_{\nu,i})}{|\tau_{2,\nu,i}|^{n+1}\exp(\zeta_\nu)}-\sum_{n=1}^{3}\sum_{m=1}^{n}\frac{\binom{3}{n}\left(\frac{\check{a}_{\nu,i}}{\check{b}_{\nu,i}}\right)^m I_m(\check{\eta}_{\nu,i})}{|\tau_{2,\nu,i}|^{n+1}\exp(\zeta_\nu)}, & \tau_{2,\nu,i}<-1\\ \sum_{n=0}^{3}\frac{-\binom{3}{n}\exp\left(\check{\zeta}_{\nu,i}-\zeta_\nu\right)}{(-\tau_{2,\nu,i})^{n+1}}\sum_{m=-n}^{\infty}\left(-\frac{\check{b}_{\nu,i}}{\check{a}_{\nu,i}}\right)^m\frac{I_{|m|}(\check{\eta}_{\nu,i})}{\exp\left(\check{\zeta}_{\nu,i}\right)}, & \tau_{2,\nu,i}>1\end{cases} \tag{31l}$$

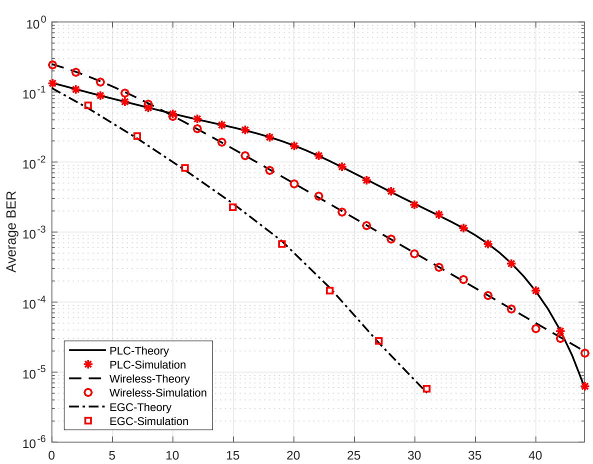

Figure 4. Average BER vs E_b/N_o in dB for DBPSK modulation for the PLC link, the wireless link, and the EGC technique.

where M_Q^S is set to 30 terms and η_Q^T is set to 20 to achieve an NRMSE less than 10^{-7}. For large arguments, the Marcum-Q function has the following asymptotic expansion [29]

$$Q\left(a,b\right) \approx \sum_{m=0}^{M_Q^L-1}\frac{b\left(-1\right)^m}{2a\sqrt{2\pi}}\left[\frac{2^{-m}\Gamma\left(\frac{1}{2}+m\right)}{m!\Gamma\left(\frac{1}{2}-m\right)} - \frac{2^{-m}\Gamma\left(\frac{3}{2}+m\right)a}{m!\Gamma\left(\frac{3}{2}-m\right)b}\right]\Phi_m,\ \eta = ab > \eta_Q^T, \tag{35}$$

where M_Q^L is set to 5 terms to achieve an NRMSE less than 10^{-7}. Φ_n can be computed recursively as $(m-1/2)\Phi_m = -(b-a)^2/(2ab)\Phi_{m-1}+\exp\left[-(b-a)^2/2\right](ab)^{-m+\frac{1}{2}}$, and $\Phi_0 = \frac{\sqrt{2\pi ab}}{b-a}\mathrm{erfc}\left[(b-a)/\sqrt{2}\right]$, where erfc(.) is the complementary error function.

Fig. 4 shows that the derived average BER expressions of the PLC link, the wireless link and the PLC/wireless EGC match the simulation results. The system parameters used to generate Fig. 4 are given in the next section.

It is worth mentioning that the BER curves presented in Figs. 3 and 4 do not follow a smooth waterfall trend as a result of the deterministic periodically-varying PLC channel. Furthermore, such a trend does not appear in the BER performance results presented in [6] for a flat PLC channel assumption under the same cyclostationary PLC noise model assumed in this paper.

VII. Numerical Results

In this section, we present numerical results for the coded BER performance of the proposed NB-PLC/wireless receive diversity combining techniques for both coherent and differential modulations. Since the average SNRs of the two links are not necessarily equal, we study the BER performance versus the variation of the average SNR of one link while fixing the average SNR of the other link. For comparison, we also study

This article has been accepted for publication in a future issue of this journal, but has not been fully edited. Content may change prior to final publication. Citation information: DOI 10.1109/TWC.2017.2697384, IEEE Transactions on Wireless Communications

Table II
PERFORMANCE GAINS OF THE PSDC TECHNIQUE OVER THE ASC TECHNIQUE AT 10^{-4} BER.

Fig.	5	6	7
Gain (dB)	3.5 dB	2.5 dB	2 dB

the BER performance for the case where both links have the same average SNR.

A. Simulation Parameters

We consider BPSK transmission in the CENELEC-A frequency band ($35.9375 - 90.6250$ kHz) for the PLC link. In addition, we assume the transmission on the wireless link to have the same bandwidth as the PLC link. The sampling rate is set to 400 kHz. We assume OFDM transmission with FFT size of 256 subchannels and a cyclic prefix of 22 samples. These parameters are chosen to be compliant with the IEEE 1901.2 NB-PLC standard.

The number of noise temporal regions for the PLC noise is $N_R = 3$ as in [14]. The ratios of the average noise powers over the three regions are $-6.59 : 1.93 : 5.15$ dB, respectively, which were obtained from the low-voltage PSD measurements in Appendix D.3 of the IEEE 1901.2 standard. The number of OFDM blocks within the noise cyclostationarity period is 13 OFDM blocks. The ratios of the time spans of the three noise regions are $\mathcal{R}_1 = 8/13$, $\mathcal{R}_2 = 3/13$ and $\mathcal{R}_3 = 2/13$. The noise on the wireless link is modeled as a GM process with $M = 2$, $\alpha_0 = 0.98$, $\alpha_1 = 0.02$ and $\sigma_1^2/\sigma_0^2 = 30$ dB. The parameters of the wireless link noise model are the same as those obtained in [17] by fitting the noise measurements in the ISM unlicensed band to a two-component Gaussian mixture PDF. E_h is set to unity for the wireless link. We assume a rate-1/2 convolutional encoding with constraint length 7 at the transmitter and a Viterbi decoder with soft decision decoding at the receiver.

We assume perfect channel knowledge at the receiver since the goal of this paper is to show the relative performance gains achieved by the investigated combining techniques rather than the absolute performance of each technique, which is a function of the implementation losses in all the blocks across the system and not just the channel estimation block. In addition, the channel estimation errors affect all the BER curves in a similar way. In other words, all BER curves (PLC, wireless and combining curves) would be shifted to the right due to the channel estimation errors. Furthermore, perfect knowledge of the average noise powers (the noise variances) of the PLC and wireless links, σ_p^2 and σ_w^2, is assumed since they can be estimated in the same way as the noise PSD is estimated, but, in this case, the averaging is performed over both OFDM blocks and frequency subchannels (both time and frequency), regardless of the noise temporal region boundaries in PLC. However, since the noise variances are scalars, they can be estimated accurately with negligible estimation errors if the averaging is long enough. In addition, the number of OFDM blocks used for PLC noise PSD estimation (which is the averaging length) is set to 4096 OFDM blocks in total (for the three noise regions). Moreover, the pilot spacing used for instantaneous noise power estimation is set to 5 subchannels.

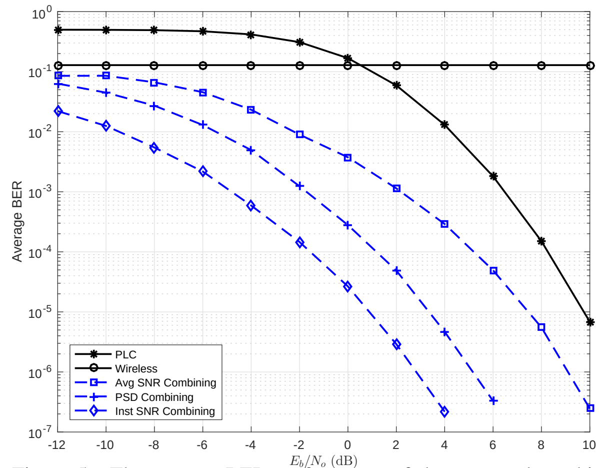

Figure 5. The average BER performance of the proposed combining techniques vs. $E_b/N_{o,p}$ at $E_b/N_{o,w} = 2$ dB.

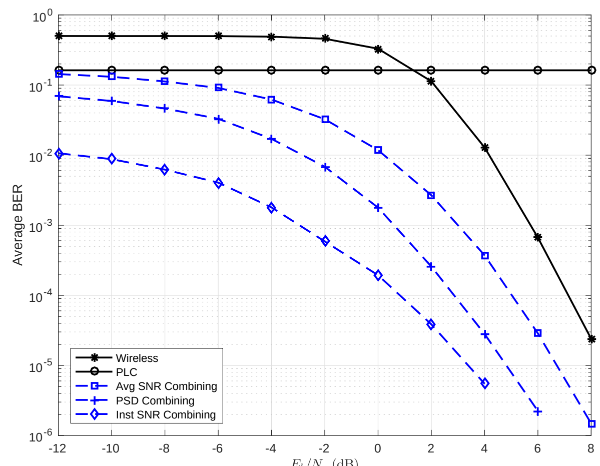

Figure 6. The average BER performance of the proposed combining techniques vs. $E_b/N_{o,w}$ at $E_b/N_{o,p} = 0$ dB.

B. Performance Results: Coherent Modulation

In this subsection, we study the average BER performance of the proposed combining techniques for the coherent modulation case. In Fig. 5, we plot the average BER versus the $E_b/N_{o,p}$ of the PLC link while fixing the $E_b/N_{o,w}$ of the wireless link at 2 dB, where $N_{o,p}$ and $N_{o,w}$ denote the noise variances for the PLC and the wireless links[3]. On the other hand, Fig. 6 depicts the average BER for both links versus the $E_b/N_{o,w}$ of the wireless link while fixing the $E_b/N_{o,p}$ of the PLC link at 0 dB. Furthermore, Fig. 7 shows the average BER of both the PLC and wireless links in case of equal $E_b/N_o = E_b/N_{o,p} = E_b/N_{o,w}$. The achieved SNR gains of the PSDC technique over the ASC technique, at a coded BER of 10^{-4}, are summarized in Table II. In addition, the SNR loss of the PSDC technique compared to the ISC technique, at a coded BER of 10^{-4}, is shown in Table III. It is worth mentioning that the pilot spacing used for instantaneous noise power estimation is 5 subchannels. From the presented performance results, we note that the PSDC technique achieves considerable SNR gains over the ASC technique at a lower

[3]For BPSK modulation, SNR is same as E_b/N_o. Hence, we use both terms interchangeably throughout this section.

This article has been accepted for publication in a future issue of this journal, but has not been fully edited. Content may change prior to final publication. Citation information: DOI 10.1109/TWC.2017.2697384, IEEE Transactions on Wireless Communications

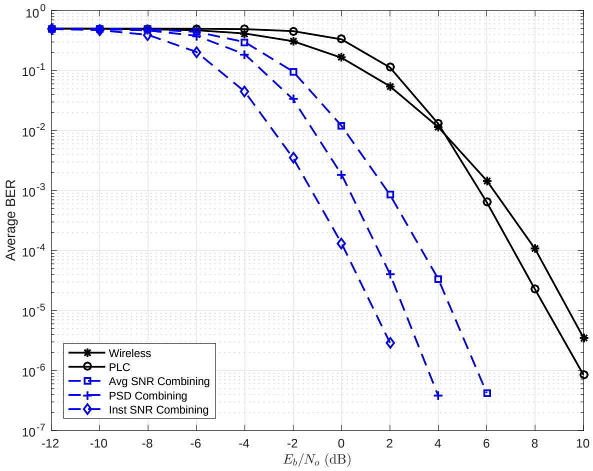

Figure 7. The average BER performance of the proposed combining techniques vs $E_b/N_o = E_b/N_{o,p} = E_b/N_{o,w}$

Table III
PERFORMANCE LOSS OF THE PSDC TECHNIQUE TO THE ISC TECHNIQUE AT 10^{-4} BER.

Fig.	5	6	7
Loss (dB)	3 dB	2 dB	1.5 dB

complexity and training overhead than the ISC technique. Hence, we conclude that the PSDC technique provides an attractive performance/complexity tradeoff.

There are two sources for the performance gains achieved by the PSDC and the ISC techniques over the performance of a single link. The first source is the scaling of the LLRs by the average SNR per subchannel in PSDC, or by the instantaneous SNR in ISC, rather than scaling the LLRs by the average SNR. This provides the decoder with a measure of the relative strength of each LLR compared to other LLRs, which enhances the decoding performance. The second source is the receive diversity combining SNR gain attained by transmitting simultaneously over two links that exhibit independent and non-identical channel and noise statistics. Figs. 8 and 9 show the performance of the PLC link and the wireless link, respectively, when the LLRs are scaled by the average SNR per subchannel (the inverse of the noise PSD) and by the instantaneous SNR. Tables IV and V quantify the SNR gains of the LLR scaling by the average SNR per subchannel and the instantaneous SNR, respectively, over scaling the LLRs by the average SNR. In addition, Tables IV and V quantify the additional SNR gains obtained from combining the LLRs of the two links over the single-link performance. It is clear from the tables that, for the PLC link, scaling the LLRs by either the average SNR per subchannel or the instantaneous SNR provides a considerable performance improvement. On the other hand, for the wireless link, scaling the LLRs by either the average SNR per subchannel or the instantaneous SNR leads to a very small performance gain.

Fig. 10 shows a comparison between the three noise power metrics, the instantaneous noise power, the average noise power per subchannel, and the average noise power, over the active frequency subchannels across multiple OFDM blocks. We note from Fig. 10 that the PSD of the noise in the wireless

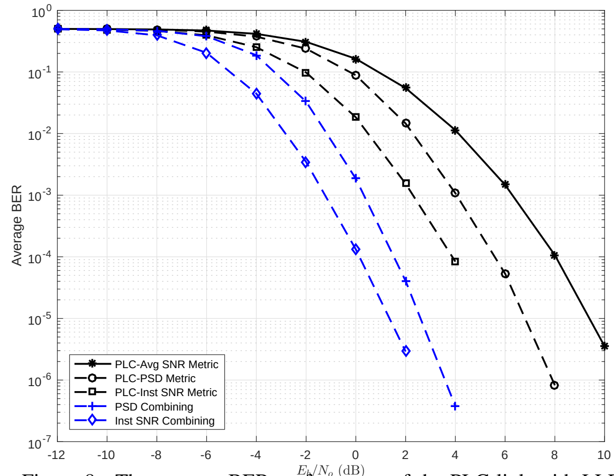

Figure 8. The average BER performance of the PLC link with LLRs scaled by the average SNR per subchannel and by the instantaneous SNR.

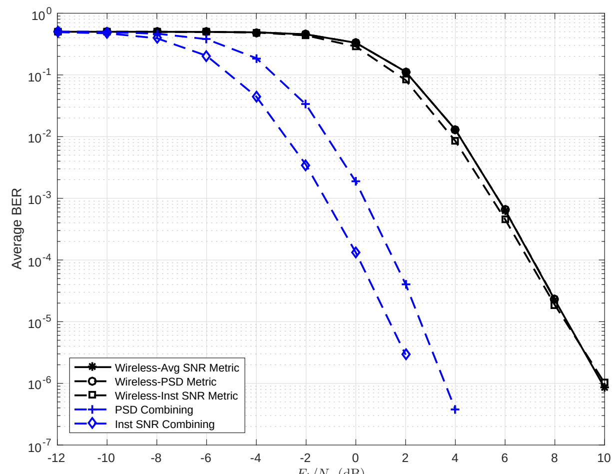

Figure 9. The average BER performance of the wireless link with LLRs scaled by the average SNR per subchannel and by the instantaneous SNR.

link is flat over frequency and equal to the GM average noise variance σ_w^2. Furthermore, it is clear from Fig. 10 that, for the wireless link, unlike the PLC link, both the instantaneous noise power and the average noise power per subchannel do not exhibit much variation around the average noise power level. Hence, for the wireless link, and specifically for our selected set of parameters for the GM noise, scaling with these metrics does not provide a significant performance gain over scaling with the average SNR. However, in scenarios where the noise on the wireless link is more impulsive, scaling the LLR with the instantaneous SNR-based metrics provides higher performance gains over scaling with the average SNR metric. This gain depends on how impulsive the GM noise is. However, the same performance is obtained using either PSD-based scaling or average noise power scaling since both are equal for GM noise.

C. Performance Results: Differential Modulations

In this section, we present performance results to compare the EGC and ASC techniques for differential modulation. As we mentioned earlier, differential modulation can be implemented over either time or frequency depending on the channel's time and frequency coherence characteristics. For

Table IV
PERFORMANCE GAINS OF PSDC OVER A SINGLE LINK AT 10^{-4} BER FOR THE CASE OF EQUAL E_b/N_o FOR BOTH LINKS.

	Gain from LLR Scaling	Diversity Combining Gain
PLC	2.5 dB	4 dB
Wireless	0.1 dB	5 dB

Table V
PERFORMANCE GAINS OF ISC OVER A SINGLE LINK AT 10^{-4} BER FOR THE CASE OF EQUAL E_b/N_o FOR BOTH LINKS.

	Gain from LLR Scaling	Diversity Combining Gain
PLC	4 dB	3.5 dB
Wireless	0.2 dB	6.5 dB

the wireless link, the channel's time variation is slow in most scenarios, as all communication terminals are fixed and the communication range is typically less than 1 km in low-density scenarios [30]. For the PLC link, the NB-PLC standards such as the IEEE 1901.2 standard, adopt FD-DM schemes since the channel variation over adjacent frequency subchannels is relatively small. Hence, in the performance results presented in this section, we focus on the case of FD-DM for the PLC link and TD-DM for the wireless link. Fig. 11 depicts the average BER performance of the ASC and the EGC techniques versus $E_b/N_{o,p}$ while fixing the $E_b/N_{o,w}$ at 4 dB. We note that the PLC and the wireless links are not symmetric in terms of their BER performance, which means that at the same E_b/N_o, the two links might have a different BER performance depending on the channel conditions and the noise parameters of each link. As a result, we note that the EGC technique outperforms the ASC technique whenever the two links have a comparable BER performance. On the other hand, the ASC technique outperforms the EGC technique whenever one link has a much better performance than the other link. For example, at high-SNR for the PLC link and low-SNR for the wireless link, the EGC technique achieves worse performance than the PLC link since it assigns equal weights to signals from both links regardless of their SNR. On the other hand, the ASC technique always shows better (or at least the same) performance than the best link since it assigns weights to the signals based on the link SNRs. Consequently, the ASC technique is a more suitable technique for PLC/wireless combining than EGC.

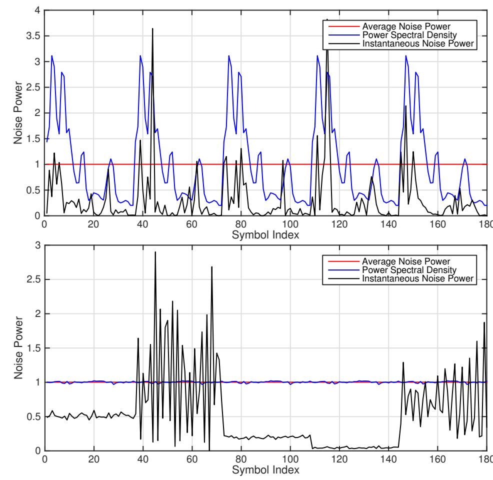

Figure 10. Comparison between noise power metrics in PLC link (top) and wireless link (down).

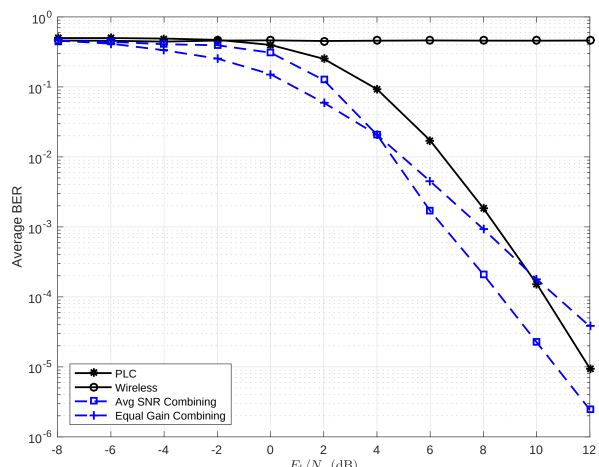

Figure 11. The average BER performance of the ASC and the EGC techniques vs $E_b/N_{o,p}$ at $E_b/N_{o,w} = 4$ dB.

VIII. CONCLUSION

Efficient receive diversity combining techniques for hybrid NB-PLC and unlicensed wireless transmission that take into account the impulsive nature of the noise and interference on both links were proposed. Furthermore, we derived closed-form expressions for the average BER performance of the proposed combining techniques and showed that they match the simulation results. In particular, for coherent modulation schemes, we compared three combining techniques with different performance/complexity tradeoffs, namely, the ASC, the PSDC and the ISC techniques. The ASC technique has the least complexity but worse performance than the PSDC and the ISC techniques. The ISC technique provides the best performance but requires a high pilot signal overhead and high complexity. The PSDC technique is shown to provide the best performance/complexity tradeoff since it achieves better performance than the ASC technique, at a lower complexity than the ISC technique. In addition, for differential modulation schemes, we compared the EGC and the ASC techniques in terms of BER performance. We showed that the ASC technique is a more suitable technique for PLC/wireless combining than the EGC technique since the ASC technique always provides a better performance, or at least the same performance, than the best link. Although the EGC technique outperforms the ASC technique if the two links have a comparable performance, the EGC technique might have worse performance than the best link when the performance of the best link is much better than the other link.

APPENDIX A

The asymptotic expansion for $\Gamma\left(\frac{1}{2}, x\right)$ is given by [25, Eq. (8.357)]

$$\Gamma\left(\frac{1}{2}, x\right) = \frac{\mathrm{e}^{-x}}{\sqrt{x}}\left[\sum_{m=0}^{M_\Gamma-1}\frac{(-1)^m\,\Gamma\left(\frac{1}{2}+m\right)}{x^m\,\Gamma\left(\frac{1}{2}\right)} + O\left(|x|^{-M_\Gamma}\right)\right]. \quad (36)$$

To evaluate the accuracy of the expansion in (36), we plot the NRMSE of the expansion, using 5 terms, i.e. $M_\Gamma = 5$, versus

This article has been accepted for publication in a future issue of this journal, but has not been fully edited. Content may change prior to final publication. Citation information: DOI 10.1109/TWC.2017.2697384, IEEE Transactions on Wireless Communications

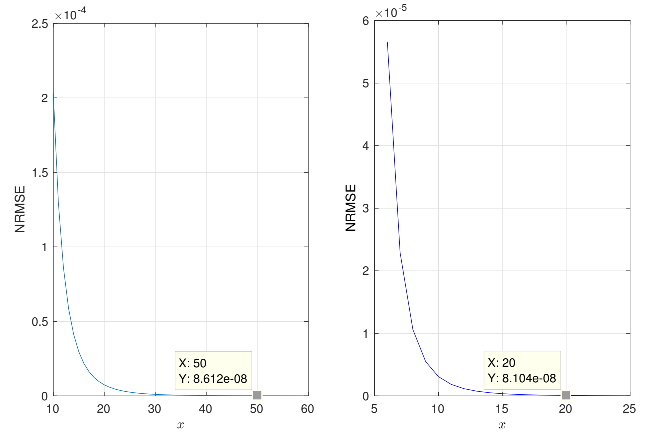

(a) NRMSE for $\Gamma\left[\frac{1}{2},x\right]$ asymptotic expansion vs. x.

(b) NRMSE for $I_0\left(x\right)$ asymptotic expansion vs. x.

Figure 12. NRMSE for the asymptotic expansions of the incomplete Gamma function and the Bessel function

the input argument x in Fig. 12(a). As clearly shown in Fig. 12(a), the NRMSE for the expansion drops to around 10^{-7} for values of the input argument greater than $\eta_{\Gamma}^{T}=50$. Hence, we use (13b) for $\eta_{k,i}^{l}$ greater than $\eta_{\Gamma}^{T}=50$.

Appendix B

The asymptotic expansion for $I_0\left(x\right)$ is given by [27, Eq. (10.40.1)]

$$I_0\left(x\right) \sim \frac{\mathrm{e}^{x}}{\sqrt{2\pi x}}\sum_{s=0}^{\infty}\frac{a_s}{s!\left(8x\right)^{s}},\ a_0=1,\ a_s=1^2 3^2\cdots \left(2s-1\right)^2,\ s\geq 1. \quad (37)$$

The NRMSE of the expansion in (37), using 5 expansion terms, is shown in Fig. 12(b) versus the input argument x. As shown in Fig. 12(b), the NRMSE for the expansion drops to around 10^{-7} for values of the input argument larger than 20. Hence, we use (37) for $\eta_{p,\nu\nu'}$ greater than $\eta_{I_0}^{T}=20$.

Appendix C

Setting $\bar{\mathbf{R}}=\bar{\mathbf{Y}}_{w,\nu\nu'}=[0,\,0]^{t}$ and $\mathbf{\Lambda}=\mathbf{\Lambda}_{w,\nu\nu'}$ in (18) results in $\alpha_1=\alpha_2=0$, and hence $a=b=0$. Thus, $P_{b,ii'}\left(E\right)$ can be written as

$$P_{b,ii'}\left(E\right)=\frac{\beta_{1,ii'}}{\beta_{1,ii'}+\beta_{2,ii'}},\ \beta_{1,ii'}=\sqrt{\omega_{ii'}^{2}+4\xi_{ii'}}-\omega_{ii'}, \quad (38a)$$

$$\beta_{2,ii'}=\sqrt{\omega_{ii'}^{2}+4\xi_{ii'}}+\omega_{ii'},\omega_{ii'}=2\tilde{E}_{b,h}\mathfrak{Re}\left(\rho\right)\xi_{ii'}, \quad (38b)$$

$$\xi_{ii'}=\frac{1}{\tilde{E}_{b,h}^{2}\left[\left(1+\bar{\gamma}_{w,i}^{-1}\right)\left(1+\bar{\gamma}_{w,i'}^{-1}\right)-|\rho|^{2}\right]}, \quad (38c)$$

where $\bar{\gamma}_{w,i}=\tilde{E}_{b,h}/\bar{\sigma}_{w,i}^{2}$, $\bar{\gamma}_{w,i'}=\tilde{E}_{b,h}/\bar{\sigma}_{w,i'}^{2}$. Inserting $\beta_{1,ii'}$ and $\beta_{2,ii'}$ into $P_{b,ii'}\left(E\right)$ yields

$$P_{b,ii'}\left(E\right)=\frac{1}{2}\left[1-\frac{1}{\sqrt{1+\frac{4\xi_{ii'}}{\omega_{ii'}^{2}}}}\right]. \quad (39)$$

Inserting the $\omega_{ii'}$ and $\xi_{ii'}$ expressions given by (38b) and (38c) into (39), we get

$$P_{b,ii'}\left(E\right)=\frac{1}{2}\left[1-\frac{1}{\sqrt{1+\mu_{w,ii'}}}\right], \quad (40a)$$

$$\mu_{w,ii'}=\frac{1}{\left[\mathfrak{Re}(\rho)\right]^{2}}\left[\left(1+\bar{\gamma}_{w,i}^{-1}\right)\left(1+\bar{\gamma}_{w,i'}^{-1}\right)-|\rho|^{2}\right]. \quad (40b)$$

Appendix D

Using the MGF of the general quadratic detector reported in [26], we can obtain the MGF of the detection metric $D_{c,\nu}$ as

$$\psi_{D_{c,\nu}}\left(v\right)=\frac{\beta_{p,\nu}^{2}\beta_{w,1,i}\beta_{w,2,i}}{\left(v-\beta_{p,\nu}\right)\left(v+\beta_{p,\nu}\right)}\times\frac{\exp\left[-A_{p,1,\nu}-\frac{A_{p,2,\nu}}{v-\beta_{p,\nu}}+\frac{A_{p,3,\nu}}{v+\beta_{p,\nu}}\right]}{\left(v-\beta_{w,1,i}\right)\left(v+\beta_{w,2,i}\right)}, \quad (41)$$

where $A_{p,1,\nu}=\alpha_{p,1,\nu}\beta_{p,\nu}^{2}$, $A_{p,2,\nu}=\beta_{p,\nu}^{2}/2(\alpha_{p,1,\nu}\beta_{p,\nu}+\alpha_{p,2,\nu})$, and $A_{p,3,\nu}=\beta_{p,\nu}^{2}/2(\alpha_{p,1,\nu}\beta_{p,\nu}-\alpha_{p,2,\nu})$. The average BER can be expressed in terms of the MGF of the detection metric as [26]

$$P_{b,\nu,i}\left(E\right)=-\frac{1}{2\pi j}\int_{-i\infty-\epsilon}^{i\infty-\epsilon}\frac{\psi_{D_{c,\nu}}\left(v\right)}{v}dv, \quad (42)$$

where ϵ is a real number chosen to move the integration path away from the singularities. Next, we use a conformal transformation from the v-plane onto the p-plane via the change of variables $p=-(\nu+\beta_{p,\nu})/(\nu-\beta_{p,\nu})$. In the p-plane, the integral given by (42) becomes

$$P_{b,\nu,i}\left(E\right)=\frac{1}{2\pi j}\int_{\Gamma_c}\frac{\frac{\beta_{w,1,i}\beta_{w,2,i}}{2p(1-p)}\exp(\frac{-\alpha_{p,1,\nu}\beta_{p,\nu}^{2}}{2})}{(\beta_{p,\nu}+\beta_{w,1,i}+(\beta_{w,1,i}-\beta_{p,\nu})p)},\times\frac{\exp(\frac{A_{p,2,\nu}}{2\beta_{p,\nu}}p+\frac{A_{p,3,\nu}}{2\beta_{p,\nu}}\frac{1}{p})\left(1+p\right)^{3}}{\left(\beta_{w,2,i}-\beta_{p,\nu}+\left(\beta_{w,2,i}+\beta_{p,\nu}\right)p\right)}dp, \quad (43)$$

where Γ_c is a positive oriented (counter-clockwise) circular contour with radius less than unity that encloses the origin, i.e. $r_c=|\Gamma_c|<1$. For the case when $\beta_{p,\nu}\neq\beta_{w,2,i}$, setting $a_{\nu}^{2}/2=A_{p,3,\nu}/\left(2\beta_{p,\nu}\right)$ and $b_{\nu}^{2}/2=A_{p,2,\nu}/\left(2\beta_{p,\nu}\right)$, (43) reduces to

$$P_{b,\nu,i}\left(E\right)=\frac{\beta_{w,1,i}\beta_{w,2,i}\exp\left(-\frac{a_{\nu}^{2}+b_{\nu}^{2}}{2}\right)}{2\left(\beta_{w,1,i}+\beta_{p,\nu}\right)\left(\beta_{w,2,i}-\beta_{p,\nu}\right)}\frac{1}{2\pi j}\int_{\Gamma_c}\times\frac{\left(1+p\right)^{3}\exp\left(\frac{a_{\nu}^{2}}{2}\frac{1}{p}+\frac{b_{\nu}^{2}}{2}p\right)dp}{p\left(1-p\right)\left(1+\tau_{1,\nu,i}p\right)\left(1+\tau_{2,\nu,i}p\right)}, \quad (44)$$

where $\tau_{1,\nu,i}=(\beta_{w,1,i}-\beta_{p,\nu})/(\beta_{w,1,i}+\beta_{p,\nu})$ and $\tau_{2,\nu,i}=(\beta_{w,2,i}+\beta_{p,\nu})/(\beta_{w,2,i}-\beta_{p,\nu})$. We note that $|\tau_{1,\nu,i}|<1$ and $|\tau_{2,\nu,i}|>1$. Hence, using partial fractions for the integrand's denominator in (44) yields

$$P_{b,\nu,i}\left(E\right)=\frac{\beta_{w,1,i}\beta_{w,2,i}}{2\left(\beta_{w,1,i}+\beta_{p,\nu}\right)\left(\beta_{w,2,i}-\beta_{p,\nu}\right)}\Big[J_{0,\nu}+c_{1,\nu,i}\times J_{1,\nu}+c_{2,\nu,i}J_{2,\nu,i}+c_{3,\nu,i}J_{3,\nu,i}\Big], \quad (45a)$$

$$J_{0,\nu}=\exp\left(-\frac{a_{\nu}^{2}+b_{\nu}^{2}}{2}\right)\sum_{k=0}^{3}\binom{3}{k}\frac{1}{2\pi j}\int_{\Gamma_c}p^{k-1}\times\exp\left(\frac{a_{\nu}^{2}}{2}\frac{1}{p}+\frac{b_{\nu}^{2}}{2}p\right)dp, \quad (45b)$$

$$J_{1,\nu}=\exp\left(-\frac{a_{\nu}^{2}+b_{\nu}^{2}}{2}\right)\sum_{k=0}^{3}\binom{3}{k}\frac{1}{2\pi j}\int_{\Gamma_c}\frac{p^{k}}{1-p}\times\exp\left(\frac{a_{\nu}^{2}}{2}\frac{1}{p}+\frac{b_{\nu}^{2}}{2}p\right)dp, \quad (45c)$$

$$J_{2,\nu,i} = \exp\left(-\frac{a_\nu^2+b_\nu^2}{2}\right)\sum_{k=0}^{3}\binom{3}{k}\frac{1}{2\pi j}\int_{\Gamma_c}\frac{p^k}{1+\tau_{1,\nu,i}p} \times \exp\left(\frac{a_\nu^2}{2}\frac{1}{p}+\frac{b_\nu^2}{2}p\right)dp, \quad (45d)$$

$$J_{3,\nu,i} = \exp\left(-\frac{a_\nu^2+b_\nu^2}{2}\right)\sum_{k=0}^{3}\binom{3}{k}\frac{1}{2\pi j}\int_{\Gamma_c}\frac{p^k}{1+\tau_{2,\nu,i}p} \times \exp\left(\frac{a_\nu^2}{2}\frac{1}{p}+\frac{b_\nu^2}{2}p\right)dp. \quad (45e)$$

To solve the integrals above, we use the following identities [26]

$$\frac{\left(\frac{b}{a}\right)^m}{2\pi j}\int_{\Gamma_c}p^{m-1}\exp\left(\frac{a^2}{2}\frac{1}{p}+\frac{b^2}{2}p\right)=\frac{\left(\frac{a}{b}\right)^m}{2\pi j}\int_{\Gamma_c}p^{-m-1} \times\exp\left(\frac{a^2}{2}\frac{1}{p}+\frac{b^2}{2}p\right)=I_m(ab), \quad (46)$$

$$\frac{1}{2\pi j}\int_{\Gamma_c}\frac{p^n}{1-p}\exp\left(\frac{a^2}{2}\frac{1}{p}+\frac{b^2}{2}p\right)=Q_1(a,b) \times\exp\left(\frac{a^2+b^2}{2}\right)-\sum_{m=0}^{n}\left(\frac{a}{b}\right)^m I_m(ab), \quad (47)$$

$$Q_1(a,b)\exp\left(\frac{a^2+b^2}{2}\right)=\sum_{m=0}^{\infty}\left(\frac{a}{b}\right)^m I_m(ab). \quad (48)$$

Using (46) and (48), $J_{o,\nu}$ and $J_{1,\nu}$, respectively, can be obtained in closed-form as shown in (31j). For $\tau_{1,\nu,i}\neq 0$, using the change of variables $|\tau_{1,\nu,i}|p=q$ in (45d), $J_{2,\nu,i}$ reduces to

$$J_{2,\nu,i} = \exp\left(-\frac{a_\nu^2+b_\nu^2}{2}\right)\sum_{k=0}^{3}\binom{3}{k}\frac{|\tau_{1,\nu,i}|^{-k-1}}{2\pi j}\int_{\hat{\Gamma}_c}q^k \times\frac{\exp\left(\frac{\hat{a}_{\nu,i}^2}{2}\frac{1}{q}+\frac{\hat{b}_{\nu,i}^2}{2}q\right)dq}{1+\mathrm{sgn}(\tau_{1,\nu,i})q}, \quad (49)$$

where sgn(.) denotes the sign function, $\hat{a}_{\nu,i}=a_\nu\sqrt{|\tau_{1,\nu,i}|}$, $\hat{b}_{\nu,i}=b_\nu/\sqrt{|\tau_{1,\nu,i}|}$ and $\hat{\Gamma}_c$ is a circular contour of radius $\hat{r}_c=r_c|\tau_{1,\nu,i}|<1$. For $-1<\tau_{1,\nu,i}<0$, where $\mathrm{sgn}(\tau_{1,\nu,i})=-1$, using (47), $J_{2,\nu,i}$ can be obtained in closed-form as shown in the first line of (31k). For $0<\tau_{1,\nu,i}<1$, since $|q|<1$, we can expand the term $1/(1+q)$ in (49) to a convergent power series and then, using (46), $J_{2,\nu,i}$ can be obtained in closed-form as shown in the second line of (31k). It is worth mentioning that for $\tau_{1,\nu,i}=0$, there is no need to evaluate $J_{2,\nu,i}$ since the factor $c_{2,\nu,i}$, which is multiplied by $J_{2,\nu,i}$ in (45a) would be equal to zero.

Since $|\tau_{2,\nu,i}|>1$, using the change of variables $1/(|\tau_{1,\nu,i}|p)=u$ in (45e), $J_{3,\nu,i}$ reduces to

$$J_{3,\nu,i} = \exp\left(-\frac{a_\nu^2+b_\nu^2}{2}\right)\sum_{k=0}^{3}\binom{3}{k}\frac{-|\tau_{2,\nu,i}|^{-k-1}}{2\pi j}\int_{\check{\Gamma}_c} \times u^{-k-1}\frac{\exp\left(\frac{\check{b}_{\nu,i}^2}{2}\frac{1}{u}+\frac{\check{a}_{\nu,i}^2}{2}u\right)du}{-\mathrm{sgn}(\tau_{2,\nu,i})-u}, \quad (50)$$

where $\check{a}_{\nu,i}=a_\nu\sqrt{|\tau_{2,\nu,i}|}$, $\check{b}_{\nu,i}=b_\nu/\sqrt{|\tau_{2,\nu,i}|}$ and $\check{\Gamma}_c$ is a circular contour of radius $\check{r}_c=1/\left(r_c|\tau_{2,\nu,i}|\right)<1$. For $\tau_{2,\nu,i}<-1$, since $|u|<1$, we can expand the term $1/(1-u)$ in (50) to a convergent power series. Thus, $J_{3,\nu,i}$ can be simplified as

$$J_{3,\nu,i} = \exp\left(-\frac{a_\nu^2+b_\nu^2}{2}\right)\sum_{k=0}^{3}\frac{\binom{3}{k}}{|\tau_{2,\nu,i}|^{k+1}}\sum_{n=0}^{\infty}\frac{-1}{2\pi j}\int_{\check{\Gamma}_c} \times u^{n-k-1}\exp\left(\frac{\check{b}_{\nu,i}^2}{2}\frac{1}{u}+\frac{\check{a}_{\nu,i}^2}{2}u\right)du. \quad (51)$$

Then, using (46), $J_{3,\nu,i}$ can be obtained as

$$J_{3,\nu,i} = \sum_{m=0}^{\infty}\frac{-\left(\frac{\check{b}_{\nu,i}}{\check{a}_{\nu,i}}\right)^m I_m(\check{a}_{\nu,i}\check{b}_{\nu,i})\exp\left(-\frac{a_\nu^2+b_\nu^2}{2}\right)}{|\tau_{2,\nu,i}|} - \sum_{k=1}^{3}\frac{\binom{3}{k}\exp\left(-\frac{a_\nu^2+b_\nu^2}{2}\right)}{|\tau_{2,\nu,i}|^{k+1}}\left[\sum_{m=1}^{k}\left(\frac{\check{a}_{\nu,i}}{\check{b}_{\nu,i}}\right)^m \times I_m(\check{a}_{\nu,i}\check{b}_{\nu,i})+\sum_{m=0}^{\infty}\left(\frac{\check{b}_{\nu,i}}{\check{a}_{\nu,i}}\right)^m I_m(\check{a}_{\nu,i}\check{b}_{\nu,i})\right] \quad (52)$$

Thus, using (48), (52) can be simplified as shown in the first line of (31l). For $\tau_{2,\nu,i}>1$, we can expand the term $1/(1+u)$ in (50) to a convergent power series and then, using (46), $J_{3,\nu,i}$ can be obtained in closed-form as shown in the second line of (31l). For the special case $\beta_{p,\nu}=\beta_{w,2,i}$, (43) reduces to

$$P_{b,\nu,i}(E) = \frac{\beta_{w,1,i}\beta_{w,2,i}\exp\left(-\frac{a_\nu^2+b_\nu^2}{2}\right)}{2\left(\beta_{w,1,i}+\beta_{p,\nu}\right)\left(\beta_{w,2,i}+\beta_{p,\nu}\right)}\frac{1}{2\pi j}\int_{\Gamma_c} \times\frac{(1+p)^3\exp\left(\frac{a_\nu^2}{2}\frac{1}{p}+\frac{b_\nu^2}{2}p\right)dp}{p^2(1-p)(1+\tau_{1,\nu,i}p)}. \quad (53)$$

Using partial fractions for the integrand's denominator in (44) yields

$$P_{b,\nu,i}(E) = \frac{\beta_{w,1,i}\beta_{w,2,i}}{2\left(\beta_{w,1,i}+\beta_{p,\nu}\right)\left(\beta_{w,2,i}+\beta_{p,\nu}\right)}\left[\tilde{c}_{0,\nu,i}J_{0,\nu} + \tilde{c}_{1,\nu,i}J_{1,\nu}+\tilde{c}_{2,\nu,i}J_{2,\nu,i}+\tilde{J}_{3,\nu}\right], \quad (54a)$$

$$\tilde{J}_{3,\nu} = \exp\left(-\frac{a_\nu^2+b_\nu^2}{2}\right)\sum_{k=0}^{3}\binom{3}{k}\frac{1}{2\pi j}\int_{\Gamma_c}p^{k-2} \times\exp\left(\frac{a_\nu^2}{2}\frac{1}{p}+\frac{b_\nu^2}{2}p\right)dp. \quad (54b)$$

Using (46), $\tilde{J}_{3,\nu}$ can be obtained in closed-form as shown in (32b).

ACKNOWLEDGEMENT

We would like to acknowledge Texas Instruments for providing field measurements for the NB-PLC noise PSD. Furthermore, we would like to thank Anand Dabak, Il-Han Kim, Tarkesh Pande and Tim Schmidl from Texas Instruments, Khurram Waheed from NXP Semiconductors, and Brian L. Evans, Ghadi Sebaali and Junmo Sung from UT Austin for useful discussions on the subject of this paper.

REFERENCES

[1] S. Galli, A. Scaglione, and Z. Wang, "For the grid and through the grid: The role of power line communications in the smart grid," *Proceedings of the IEEE*, vol. 99, no. 6, pp. 998–1027, 2011.

[2] M. Nassar, J. Lin, Y. Mortazavi, A. Dabak, I. H. Kim, and B. L. Evans, "Local utility power line communications in the 3–500 kHz band: channel impairments, noise, and standards," *IEEE Signal Processing Magazine*, vol. 29, no. 5, pp. 116–127, 2012.

[3] J. Lin, M. Nassar, and B. L. Evans, "Impulsive noise mitigation in powerline communications using sparse Bayesian learning," *IEEE Journal on Selected Areas in Communications*, vol. 31, no. 7, pp. 1172–1183, 2013.

[4] M. Sayed and N. Al-Dhahir, "Narrowband-PLC/wireless diversity for Smart Grid communications," in *Proc. IEEE GLOBECOM*, Austin, TX, USA, Dec. 2014.

[5] M. Sayed, I.-H. Kim, T. Pande, A. Batra, and N. Al-Dhahir, "Proposed frame and preamble structure for MIMO narrowband power line communications," in *Proc. IEEE ISPLC*, Austin, TX, USA, Mar./Apr. 2015, pp. 65–70.

[6] M. Sayed, G. Sebaali, B. L. Evans, and N. Al-Dhahir, "Efficient diversity technique for hybrid narrowband-powerline/wireless smart grid communications," in *Proc. IEEE SmartGridComm*, Miami, FL, USA, Nov. 2015, pp. 1–6.

[7] M. Elgenedy, M. Sayed, M. Mokhtar, M. Abdallah, and N. Al-Dhahir, "Interference mitigation techniques for narrowband powerline smart grid communications," in *Proc. IEEE SmartGridComm*, Miami, FL, USA, Nov. 2015, pp. 368–373.

[8] M. Nassar and B. L. Evans, "Low complexity EM-based decoding for OFDM systems with impulsive noise," in *Proc. IEEE 45th ASILOMAR*, Pacific Grove, CA, USA, Nov. 2011, pp. 1943–1947.

[9] W. Sun, M. Choi, and S. Choi, "IEEE 802.11ah: A long range 802.11 WLAN at sub 1 GHz," *Journal of ICT Standardization*, vol. 1, no. 1, pp. 83–108, 2013.

[10] E. Khorov, A. Lyakhov, A. Krotov, and A. Guschin, "A survey on IEEE 802.11 ah: An enabling networking technology for smart cities," *Computer Communications*, vol. 58, pp. 53–69, 2015.

[11] T. Adame, A. Bel, B. Bellalta, J. Barceló, J. Gonzalez, and M. Oliver, "Capacity analysis of IEEE 802.11 ah WLANs for M2M communications," in *International Workshop on Multiple Access Communications*, 2013, pp. 139–155.

[12] S. Lai and G. Messier, "Using the wireless and PLC channels for diversity," *IEEE Transactions on Communications*, vol. 60, no. 12, pp. 3865–3875, 2012.

[13] S. W. Lai, N. Shabehpour, G. G. Messier, and L. Lampe, "Performance of wireless/power line media diversity in the office environment," in *Proc. IEEE GLOBECOM*, Austin, TX, USA, 2014, pp. 2972–2976.

[14] M. Nassar, A. Dabak, I. H. Kim, T. Pande, and B. L. Evans, "Cyclostationary noise modeling in narrowband powerline communication for smart grid applications," in *Proc. IEEE ICASSP*, Kyoto, Japan, Mar. 2012, pp. 3089–3092.

[15] "Key Priorities for Sub-GHz Wireless Deployment." [Online]. Available: http://www.silabs.com/Support\%20Documents/TechnicalDocs/Key-Priorities-for-Sub-GHz-Wireless-Deployments.pdf

[16] "Sub-Ghz vs 2.4 GHz: Which one to choose?" [Online]. Available: https://community.nxp.com/thread/330069

[17] M. Nassar, "Graphical models and message passing receivers for interference limited communication systems," Ph.D. dissertation, University of Texas at Austin, 2013.

[18] A. Nasri and R. Schober, "Performance of BICM-SC and BICM-OFDM systems with diversity reception in non-Gaussian noise and interference," *IEEE Transactions on Communications*, vol. 57, no. 11, pp. 3316–3327, 2009.

[19] W. Liu, M. Sigle, and K. Dostert, "Channel characterization and system verification for narrowband power line communication in smart grid applications," *IEEE Communications Magazine*, vol. 49, no. 12, pp. 28–35, 2011.

[20] N. Shlezinger and R. Dabora, "On the capacity of narrowband PLC channels," *IEEE Transactions on Communications*, vol. 63, no. 4, pp. 1191–1201, 2015.

[21] J. Häring and A. J. H. Vinck, "Performance bounds for optimum and suboptimum reception under class-A impulsive noise," *IEEE Transactions on Communications*, vol. 50, no. 7, pp. 1130–1136, 2002.

[22] N. Shlezinger and R. Dabora, "Frequency-shift filtering for OFDM signal recovery in narrowband power line communications," *IEEE Transactions on Communications*, vol. 62, no. 4, pp. 1283–1295, 2014.

[23] M. Sayed, T. A. Tsiftsis, and N. Al-Dhahir, "Appendix for "On the Diversity of Hybrid Narrowband-PLC/Wireless Communications for Smart Grids"." [Online]. Available: https://www.researchgate.net/publication/313770341_Appendix_for_On_the_Diversity_of_Hybrid_Narrowband-PLCWireless_Communications_for_Smart_Grids

[24] J. G. Proakis, *Digital communications*, 5th ed. New York, NY, USA: McGraw-Hill, 2008.

[25] I. S. Gradshtein and I. M. Ryzhik, *Table of integrals, series, and products*, 7th ed. New York, NY, USA: Academic Press, 2007.

[26] J. Proakis, "On the probability of error for multichannel reception of binary signals," *IEEE Transactions on Communication Technology*, vol. 16, no. 1, pp. 68–71, 1968.

[27] F. W. Olver, *NIST Handbook of Mathematical Functions*. Cambridge University Press, 2010.

[28] P. C. Sofotasios, T. A. Tsiftsis, Y. A. Brychkov, S. Freear, M. Valkama, and G. K. Karagiannidis, "Analytic expressions and bounds for special functions and applications in communication theory," *IEEE Transactions on Information Theory*, vol. 60, no. 12, pp. 7798–7823, 2014.

[29] A. Gil, J. Segura, and N. M. Temme, "Algorithm 939: Computation of the Marcum Q-function," *ACM Transactions on Mathematical Software (TOMS)*, vol. 40, no. 3, p. 20, 2014.

[30] C.-S. Sum, M. A. Rahman, L. Lu, F. Kojima, and H. Harada, "On communication and interference range of IEEE 802.15. 4g smart utility networks," in *Proc. IEEE WCNC*, Paris, France, Apr. 2012, pp. 1169–1174.

Mostafa Sayed (S'13) was born in Giza, Egypt. He received the B.Sc. and M.Sc. degrees in electrical engineering from Cairo University, Giza, Egypt, in 2008 and 2013, respectively. He is currently working towards his Ph.D. degree in electrical engineering at the University of Texas at Dallas, Richardson, TX, USA. From 2008 to 2013, he was a System Design Engineer at Varkon (Wasiela) Semiconductors, Cairo, Egypt, where he worked on the design of hardware-oriented digital signal processing algorithms for wireless communications receivers. He was an intern at Texas Instruments, Dallas, TX during Summer 2014 and Summer 2015, where he worked on PHY layer algorithm design for low-power power line and wireless Smart Grid communications. His current research interests include Smart Grid communications, design of wireless and power line communication systems, and implementation of hardware efficient signal processing algorithms.

Theodoros A. Tsiftsis (S'02, M'04, SM'10) was born in Lamia, Greece, in 1970. He received the B.Sc. degree in physics from the Aristotle University of Thessaloniki, Greece, in 1993, the M.Sc. degree in digital systems engineering from the Heriot-Watt University, Edinburgh, U.K., in 1995, the M.Sc. degree in decision sciences from the Athens University of Economics and Business, in 2000, and the Ph.D. degree in electrical engineering from the University of Patras, Greece, in 2006. He joined the Technological Educational Institute of Central Greece, in 2010. He is currently an Associate Professor of communication technologies with the School of Engineering, Nazarbayev University, Astana, Kazakhstan. He has authored or co-authored over 120 technical papers in scientific journals and international conferences. His research interests include the broad areas of cooperative communications, cognitive radio, communication theory, wireless powered communication systems, and optical wireless communication systems. Dr. Tsiftsis acts as a Reviewer for several international journals and conferences. He has served as Senior or Associate Editor in the Editorial Boards of IEEE TRANSACTIONS ON VEHICULAR TECHNOLOGY and IEEE COMMUNICATIONS LETTERS. He is currently an Area Editor for Wireless Communications II of the IEEE TRANSACTIONS ON COMMUNICATIONS and an Associate Editor of the IEEE TRANSACTIONS ON MOBILE COMPUTING.

Naofal Al-Dhahir is Erik Jonsson Distinguished Professor at UT-Dallas. He earned his PhD degree in Electrical Engineering from Stanford University. From 1994 to 2003, he was a principal member of the technical staff at GE Research and AT&T Shannon Laboratory. He is co-inventor of 41 issued US patents, co-author of over 350 papers and co-recipient of 4 IEEE best paper awards. He is the Editor-in-Chief of IEEE Transactions on Communications and an IEEE Fellow.